APPLICATION OF AUTOREGRESSIVE MOVING AVERAGE LINEAR PREDICTION FILTERS TO THE CHARACTERIZATION OF SOLAR WIND-MAGNETOSPHERE COUPLING

THESIS

Carter N. Borst, Captain, USAF
AFIT/GAP/ENP/95D-01

DEPARTMENT OF THE AIR FORCE
AIR UNIVERSITY
AIR FORCE INSTITUTE OF TECHNOLOGY

Wright-Patterson Air Force Base, Ohio

AFIT/GAP/ENP/95D-01

APPLICATION OF AUTOREGRESSIVE MOVING AVERAGE LINEAR PREDICTION FILTERS TO THE CHARACTERIZATION OF SOLAR WIND-MAGNETOSPHERE COUPLING

THESIS

Carter N. Borst, Captain, USAF
AFIT/GAP/ENP/95D-01

REPORT DOCUMENTATION PAGE

Form Approved
OMB No. 0704-0188

1. AGENCY USE ONLY *(Leave blank)*	2. REPORT DATE	3. REPORT TYPE AND DATES COVERED
	January 1996	Master's Thesis

4. TITLE AND SUBTITLE
Application of Autoregressive Moving Average Linear Prediction Filters to the Characterization of Solar Wind-Magnetosphere Coupling

5. FUNDING NUMBERS

6. AUTHOR(S)
Carter N. Borst, Capt, USAF

7. PERFORMING ORGANIZATION NAME(S) AND ADDRESS(ES)
Air Force Institute of Technology, WPAFB OH 45433-6583

8. PERFORMING ORGANIZATION REPORT NUMBER

9. SPONSORING / MONITORING AGENCY NAME(S) AND ADDRESS(ES)
Ed Cliver
PL/GPSG
29 Randolph Rd
Hanscom AFB, MA 01731-3010

10. SPONSORING / MONITORING AGENCY REPORT NUMBER

11. SUPPLEMENTARY NOTES

12a. DISTRIBUTION / AVAILABILITY STATEMENT
Approved for public release; distribution unlimited

12b. DISTRIBUTION CODE

13. ABSTRACT *(Maximum 200 words)*

Linear prediction filtering techniques have been used in studying the coupling processes between the solar wind and magnetosphere. The magnetosphere is a complex, dynamic system with at least two independent coupling methods for energy input, driven and unloading. Linear models were built and tested on the Bargatze data set, consisting of over 70 days of geomagnetic indices and solar wind data ordered in 34 intervals of increasing geomagnetic activity. Linear filtering techniques employing single- and multiple-input, autoregressive models predicted values of the magnetic index AL from solar wind data. The impulse response curves of the AL-coupling function groups showed amplitude peaks at 25 and 70 minutes, confirming results in previous studies. The separate peaks indicate responses corresponding to the driven and unloading time scales. The average correlation coefficients generated between predicted AL values and the measured values of AL were 0.665, 0.738, and 0.793 for single, dual, and triple input models, respectively.

14. SUBJECT TERMS	15. NUMBER OF PAGES
Magnetosphere, Solar wind, Geomagnetic activity, Prediction filters Linear filters, magnetospheric coupling	104
	16. PRICE CODE

17. SECURITY CLASSIFICATION OF REPORT	18. SECURITY CLASSIFICATION OF THIS PAGE	19. SECURITY CLASSIFICATION OF ABSTRACT	20. LIMITATION OF ABSTRACT
Unclassified	Unclassified	Unclassified	UL

AFIT/GAP/ENP/95D-01

APPLICATION OF AUTOREGRESSIVE MOVING AVERAGE LINEAR PREDICTION FILTERS TO THE CHARACTERIZATION OF SOLAR WIND-MAGNETOSPHERE COUPLING

THESIS

Presented to the Faculty of the School of Engineering

Air Education and Training Command

In Partial Fulfillment of the

Requirements for the Degree of

Master of Science in Applied Physics

Carter N. Borst

Captain, USAF

December 1995

AFIT/GAP/ENP/95D-01

APPLICATION OF AUTOREGRESSIVE MOVING AVERAGE LINEAR PREDICTION FILTERS TO THE CHARACTERIZATION OF SOLAR WIND-MAGNETOSPHERE COUPLING

Carter N. Borst
Captain, USAF

Approved:

Wm. F. Bailey — 1 Dec 95
Dr. William F. Bailey

Derrill J. Goldizen — 1 Dec 1995
Dr. Derrill Goldizen

David Weeks — Dec 1, 1995
Dr. David Weeks

Acknowledgments

I would like to thank Karyl, Roy, Matt, Gordon, Charlie, and Clark who shared their knowledge of the UNIX system and suggestions. Also, thank you for not exiling me from the back-room computer area for all of my tirades, arguments with the computer, and assorted noises.

Thanks to my mom and dad and Randal for support given over the phone lines. It really did matter.

Many, many thanks to the actual researchers in the field who took time out of their busy schedules to answer some of my sillier questions and provide me with data which turned out to be invaluable. They are: Ed Cliver, Don Smart, Alexander Klimas, and those who pointed me in their direction.

Thank you Derrill for taking time out of your schedule to read my attempts, make suggestions, and point me in the right (general) direction. From all appearances, neither of our times were wasted.

Finally, my greatest thanks to Dr. William F. Bailey, my advisor. Most of the time I think you thought I knew more. Thank you for all of the guidance and kicks in the pants to jump-start my brain.

Carter N. Borst

Table of Contents

Page

List of Equations

List of Figures

List of Figures (cont)

Figure Page

List of Tables

Abstract

Linear prediction filtering techniques have been used in studying the coupling processes between the solar wind and magnetosphere. The magnetosphere is a complex, dynamic system with at least two independent coupling methods for energy input, driven and unloading. Linear models were built and tested on the Bargatze data set, consisting of over 70 days of geomagnetic indices and solar wind data ordered in 34 intervals of increasing geomagnetic activity. Linear filtering techniques employing single- and multiple-input, autoregressive models predicted values of the magnetic index AL from solar wind data. The impulse response curves of the AL-coupling function groups showed amplitude peaks at 25 and 70 minutes, confirming results in previous studies. The separate peaks indicate responses corresponding to the driven and unloading time scales. The average correlation coefficients generated between predicted AL values and the measured values of AL were 0.665, 0.738, and 0.793 for single, dual, and triple input models, respectively.

APPLICATION OF AUTOREGRESSIVE MOVING AVERAGE LINEAR PREDICTION FILTERS TO THE CHARACTERIZATION OF SOLAR WIND-MAGNETOSPHERE COUPLING

I. Introduction

Background

In the last three decades of solar wind-magnetosphere coupling research, geomagnetic activity has been indirectly linked to variations in the solar wind. In general, changes in components of the solar wind (bulk solar wind speed, Interplanetary Magnetic Field (IMF) strength and orientation, etc.) cause changes in the geomagnetic activity levels. The exact relation defining the interaction between the solar wind and the magnetosphere is currently unknown. Several theories have been proposed, but none are able to account for all of the observed phenomena.

Due to the complexity of the detailed physical relationship between solar wind components and geomagnetic activity levels, empirical techniques have been used to relate the two. Correlative studies [Gonzalez, 1990] have established "important" solar wind parameters. When adopted as "inputs" in a linear predictive filter analysis [Bargatze et al., 1985; Clauer, 1986] or "states" in a state-input space approach [Vassiliadis et al., 1995], geomagnetic activity, in terms of the magnetic indices, may be forecast with a high degree of success. These system approaches additionally provide insight on energy

transfer/relaxation time scales and permit assessment of simple models of solar wind-magnetosphere coupling.

The solar wind is an extension of the Sun's corona. The Sun's activity, and hence the solar wind's characteristics, are primarily chaotic in nature, with only a minimum of its features being predictable. If a forecast of the geomagnetic indices is desired, solar wind data retrieved from a point upstream of the Earth (nearer to the Sun) is required. The WIND/Solar Wind Interplanetary Measurements (WIND/SWIM) satellite, launched by National Aeronautics and Space Administration (NASA) in November of 1994, provides data on the components of the solar wind (Figure 1). In May 1997, the satellite will enter a permanent orbit at the Lagrange point, named "L1", located at approximately 1% of the Sun-Earth distance upstream. From this distance, data recorded by the satellite provides researchers approximately one hour lead time before coupling actions are initiated between the solar wind and magnetosphere.

Problem Statement

The 50th Weather Squadron (50 WS), located at Falcon AFB in Colorado Springs, prepares and disseminates forecasts and information on the solar and geomagnetic activity levels. The standard forecast is persistence, i.e., forecasting current conditions to continue into the future. The 50 WS has currently begun implementing and testing the Magnetospheric Specification Model (MSM), a model that describes the current state of the magnetosphere. The model uses various inputs but can be run with a single input, the magnetic index Kp.

In the near future, the Magnetospheric Specification Forecast Model (MSFM) will begin testing. Until the MSFM (a true forecast model) is fully implemented, the MSM (a "nowcast" model) using a predicted Ap will provide the only predictive capability to the forecasters. Thus, the development of a model which can predict Ap would greatly enhance the capability of the MSM and provide a better prediction of geomagnetic activity than persistence.

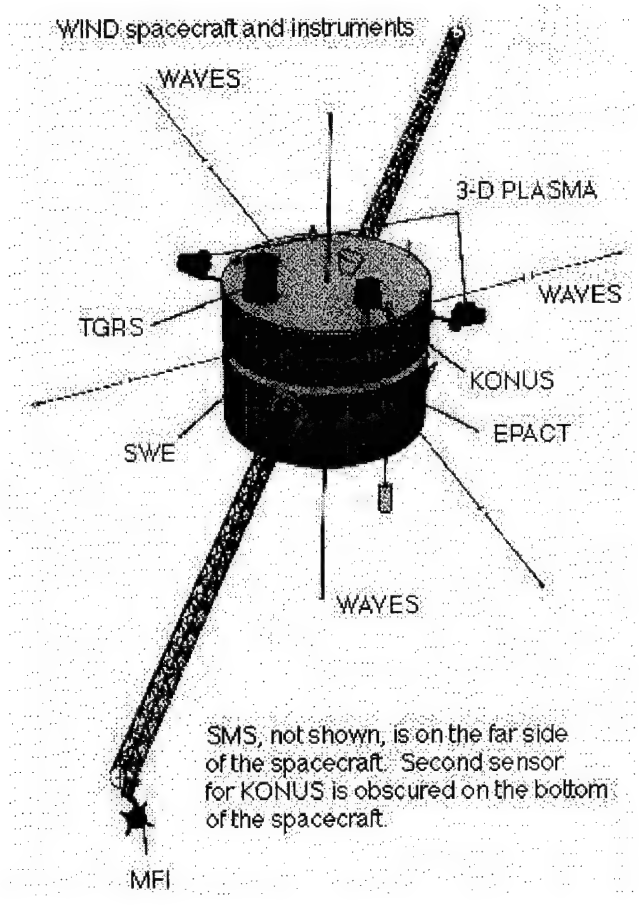

Figure 1. WIND/SWIM Satellite. (Courtesy of the Space Environment Lab, Boulder.)

Research Objectives

The initial research objective of this thesis will be to reproduce the results of Clauer [1986], applying linear prediction filter techniques to solar wind-magnetosphere coupling. Specifically, using the Bargatze data set [Bargatze, 1985], a 5-interval, moving-average filter will be constructed to predict AL from VB_S, the product of the bulk solar wind speed and the rectified vertical component of the solar wind's magnetic field.

The results will be compared with previous works and actual measurements of the AL index. Multiple input models will then be developed to determine possible improvement in the predictive capability of linear filter models. The results of the multiple input models will then be contrasted with a state-input space model [Vassiliadis, 1995].

Data Source

The data base for this study will be the Bargatze data set. This data set is comprised of data recorded from November 1973 to December 1974 and is the same data set used by Clauer [1986] and Vassiliadis, et al. [1995]. The data set consists of the AL and AE indices as well as solar wind plasma and IMF measurements at 2.5 minute time resolution. The plasma and IMF observations were averaged over 2.5 minute periods for comparison with the AL index values, which were obtained from the World Data Center, Boulder, Colorado [Clauer, 1986].

There are 34 time intervals included in the Bargatze data set, ordered from low- to high-level activity, and encompassing 73 days of data. The intervals are at least one day

long, but shorter than four days. Each interval is temporally bounded at both ends by a 2-hour segment of small, nearly zero solar wind input and AL index values [Bargatze, 1985].

II. Literature Review

In this chapter, the relevant background information will be given in five sections. The first section will discuss the physics of the solar wind, magnetosphere, and solar wind-magnetosphere coupling. The second portion will introduce the relevant geomagnetic indices, discuss how they are formed, and identify the geographic latitudes where their areas of greatest influence lie. The third section will give a more detailed description of the WIND/SWIM satellite. The fourth section will review the approaches and findings of Bargatze et al. [1985], Clauer [1986], and Vassiliadis et al. [1995]. The last section will introduce and explain the criteria for assessing the quality and accuracy of the overall output.

Solar Wind and Magnetosphere

The sun's atmosphere does not have a well-defined exterior boundary. The solar corona expands into space, and is referred to as the solar wind. The solar wind is a fully-ionized, quasi-neutral plasma, consisting primarily of electrons and protons, but including some traces of heavier ionized particles [Parks, 1991]. The solar wind plasma, by definition an excellent conductor, carries the corona's magnetic field with it as it leaves the sun's atmosphere. As the solar wind convects outward to space, it stretches the sun's open magnetic field lines outward, creating the IMF [Tascione, 1994].

The solar wind's parameters, i.e., the bulk velocity, IMF strength, and IMF orientation, are the primary determinants of geomagnetic activity. Characteristic values

of the bulk velocity and IMF strength range between 300 and 1000 $km \cdot s^{-1}$ and ones to tens of nanotesla for the vertical component, respectively. The values of the horizontal IMF components are much stronger, ranging from tens to a few hundred nanotesla. These variations occur primarily because of Coronal Mass Ejections (CME), Coronal Holes (CH), and solar flares. Solar flares and CMEs are sporadic in nature and provide short-lived bursts of energy to the solar wind. Coronal holes are relatively long-lived features, and may influence geomagnetic activity for several solar rotations [Tascione, 1994]. High solar wind speed, high IMF strength, and southward-oriented IMF field lines are, in combination or individually, the major causes for the largest variations in geomagnetic activity, geomagnetic storms.

Geomagnetic storms are divided into 2 primary classes: substorms and major storms. Substorms occur on a time scale of 1 to 3 hours and are generally less than half as intense as the major storms. The major storms are typically longer in duration, lasting from 3 hours to 7 days, with intensities, expressed in terms of magnetic deviations from the norm, averaging larger than -50 nT (where the more negative the measurement of the storm is, the greater its strength). The true source of a substorm is still unresolved; however, some causes ascribed in current theories are a sudden change of orientation in IMF from northward to southward, a sharp change in solar wind speed or density, or even a spontaneous event with no apparent cause [Hargreaves, 1992:200]. Major storms are almost always related to significant activity on the surface of the Sun. Sunspot groups, large coronal holes, and high solar flare activity over an extended period of time are some causes of major storms and high geomagnetic activity.

The solar wind experiences fluid-like shocks, due to acceleration of the plasma as it leaves the solar corona. This was first proposed in E.N. Parker's dynamic model of the sun and solar wind [Parker, 1958]. The speed of the solar wind averages approximately 400 $km \cdot s^{-1}$, which is 5 to 10 times greater than supersonics speeds in space. As the solar wind expands radially, a slow-moving region may be compressed by a fast-moving region ejected after it. The diffusion of magnetic fields between the regions does not occur over the time they take to reach the Earth, so a discontinuity develops between the fast- and slow-moving regions. As there are no actual collisions between particles or the regions containing them, the shocks are termed collisionless [Parks, 1991:5]. It is through collisionless interactions that the energy stored in magnetic fields is transferred to the plasma.

The magnetosphere's shape is the result of the interaction between the Earth's magnetic field and the solar wind (Figure 2). As the solar wind streams past, it pushes (via magnetic pressure) and couples with the Earth's magnetic field lines (via magnetic field line merging) allowing the solar wind's energy to be transferred to the magnetosphere. This is why the shape of the Earth's magnetosphere is asymmetric, a small bubble on the sunward side, upstream, and an extended tail in the anti-sunward direction, downstream.

For the purposes of this thesis, the relevant features of the magnetosphere are: the bow shock, magnetopause, plasmasphere, magnetotail, and the cusps. Distance measurements in the magnetosphere are usually in units of Earth radii (R_E). The bow

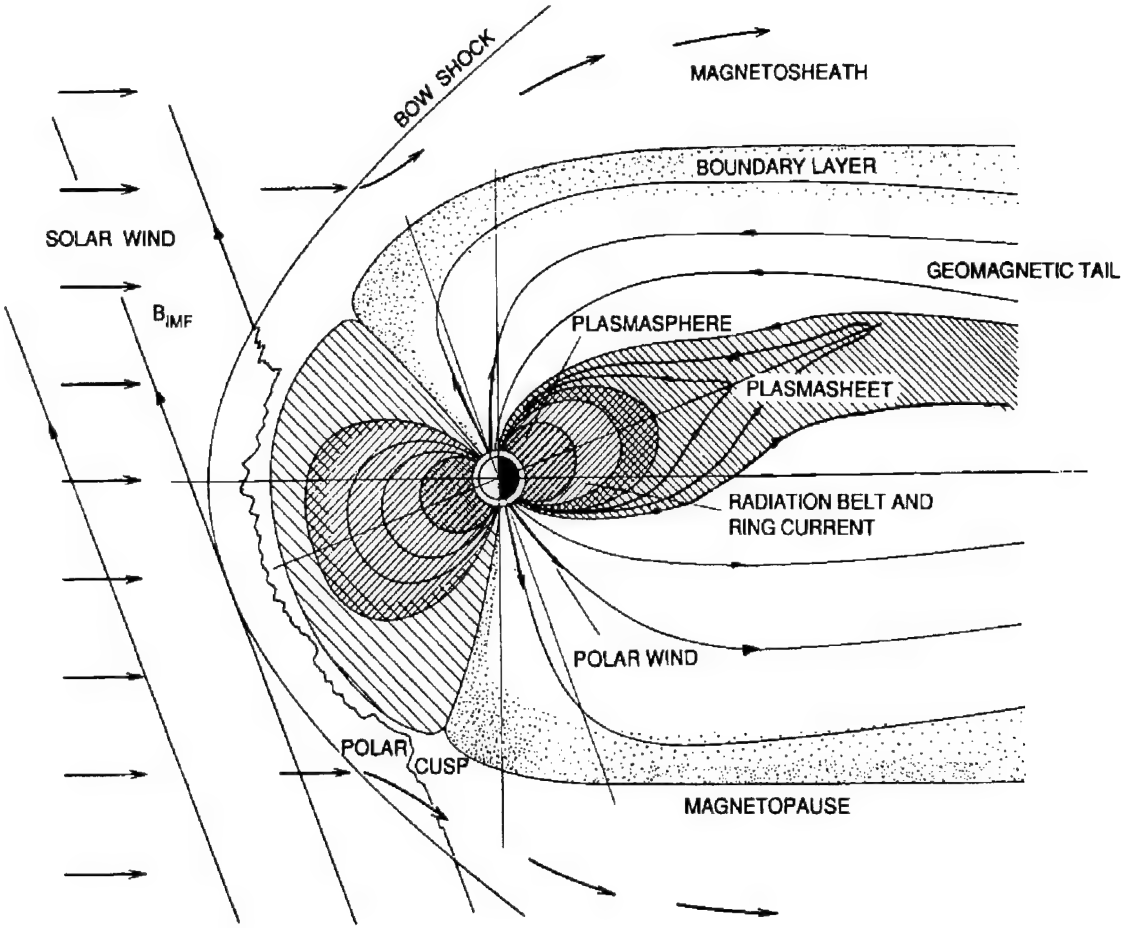

Figure 2. The Earth's Magnetosphere.
(Parks [1991:8])

shock is understood to be similar in nature to an aerodynamic shock ahead of a blunt body. The solar wind cannot pass through the magnetosphere so it must slow down, transfer energy to the magnetosphere, and then be pushed around it by the subsequent solar wind. The magnetopause is the boundary between the solar wind and the magnetosphere and is generally located at 10 R_E upstream of Earth. The plasmasphere is the lower portion of the magnetosphere surrounding Earth (3 to 4 R_E) which corotates with the neutral atmosphere and ionosphere. The cusps (or clefts) are narrow regions encompassing magnetic field lines open to the solar wind plasma and extending down from the high latitude magnetopause to the polar ionosphere. They indicate the primary areas for solar wind plasma injection into the ionosphere.

There are also current systems in the magnetosphere. These currents are generated as the ions and electrons traveling along the magnetopause boundary or within the magnetosphere slowly drift across geomagnetic field lines. The variations in the magnetospheric current systems (which the geomagnetic indices reflect) affect the current systems in the ionosphere. Figures 3 and 4 show the major magnetospheric current systems and their effects on the current systems of the Earth's ionosphere.

The magnetospheric current systems are: the magnetopause current, ring current, neutral (or cross-tail) current sheet, and the field-aligned current. The current found at the magnetopause is created by the amount of mass and energy transmitted across the magnetopause. According to Tascione [1994], observations of this boundary indicate that approximately 0.5% of the solar wind's mass incident on the dayside of the magnetosphere

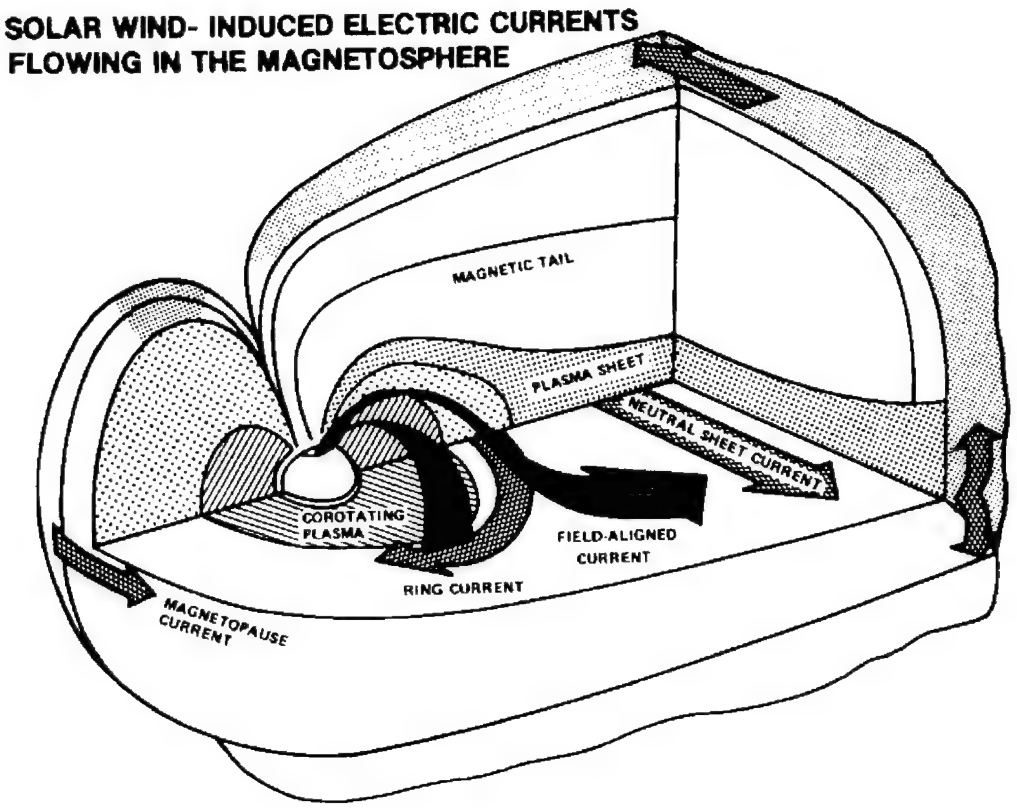

Figure 3. The magnetospheric current system. (Parks [1991: 244])

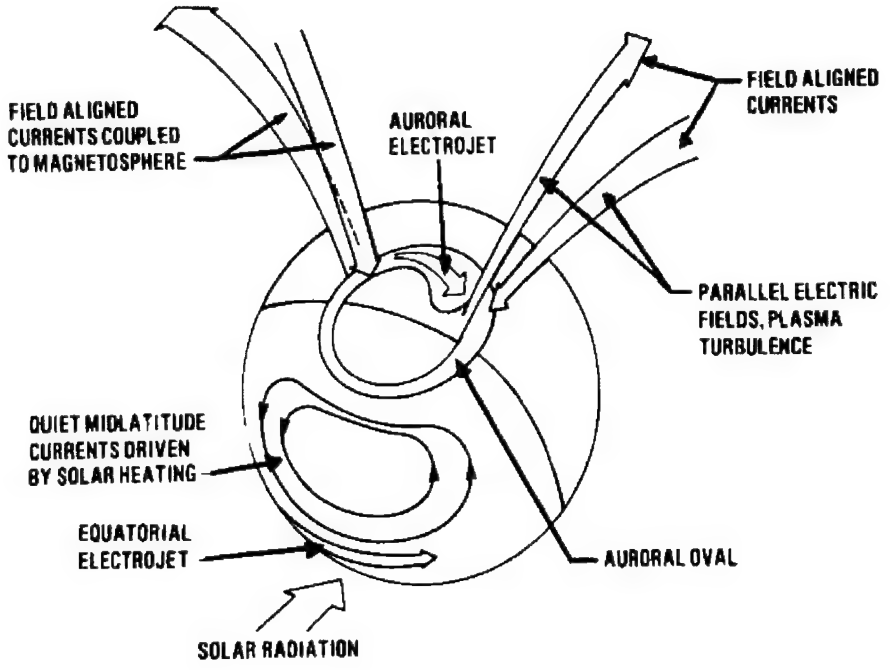

Figure 4. The ionospheric current system. (Parks [1991:244])

passes through the magnetopause. The ring current encircles the geomagnetic equator, and is typically located between 3 to 6 R_E. It involves a slow drift of particles across the magnetic field lines. The neutral sheet current system separates the oppositely directed magnetic fields emanating from the north and south polar caps. The undisturbed neutral sheet is about 5 R_E thick and has an identifiable inner edge near 7 R_E on the anti-sunward side The field-aligned currents (also called Birkeland currents) flow parallel to the Earth's magnetic field into the high-latitude auroral oval. These currents produce a magnetic perturbation in a direction perpendicular to the Earth's magnetic field and generate a small current by

$$\mu_O \mathbf{J}_{||} = (\nabla \times \delta\mathbf{B})_{||} \qquad (1)$$

where μ_O is the magnetic permeability of free space, $\mathbf{J}_{||}$ is the Birkeland current density, and $\delta\mathbf{B}$ is the magnetic perturbation perpendicular to the Earth's magnetic field [Kelley, 1989:296-7]. The magnetic perturbation which creates the small field aligned currents also produces a convective electric field, according to Maxwell's equations. The electric field can be mapped into the ionosphere or back out into the magnetosphere, i.e. the field aligned currents may be driven by the actions of the ionosphere or the magnetosphere. This interactive relationship is why Birkeland currents are an essential link between the solar wind-magnetosphere system and the ionospheric system [Kelley, 1989:296-7].

These two current systems, the magnetospheric and ionospheric, have a great deal of influence on the time scale and intensity of geomagnetic activity. The magnetospheric system responds much quicker to the solar wind inputs than the ionospheric current system. The enhanced response time is due to the immediate coupling of the southward

IMF and the Earth's magnetic field, resulting in the erosion of the Earth's field when the IMF turns southward. The majority of the energy from the solar wind is "loaded" into the magnetosphere in this time. This mechanism has been termed the driven model for solar wind-magnetosphere coupling because these parameters directly drive the reaction of the magnetosphere. A second mechanism, associated with the unloading model, requires the energy input to be stored in the magnetotail, and later released to modify the current systems. The response time of the unloading model is on the order of 8 hours. When the magnetotail releases the stored energy, it is in the form of precipitated particle injection into the ring current or auroral electrojet. This unloading response is consistently apparent for all of the input parameters used in this study, and will be discussed further using the parameter VB_S, which describes the convective electric field and is closely related to the current system.

The orientation of the IMF field is considered to be the most important factor when determining the occurrences of geomagnetic storms. Southward-oriented IMF are thought to couple with the Earth's magnetic field lines and allow them to be swept back into the magnetotail (Figure 5). When this occurs, the magnetosphere erodes as the solar wind moves into the regions where the magnetic field lines and magnetospheric particles have been evacuated.

> "The energy transfer or coupling process begins when enhanced magnetic merging is initiated on the dayside magnetopause. The process ends when the energy is irreversibly dissipated by auroral particle precipitation, Joule heating in the ionosphere, or particle injection into the ring current and when energy is lost from the magnetosphere via plasmoid formation" [Bargatze et al., 1985:6387].

Baumjohann [1986] states "...magnetic merging is the dominant coupling process and provides roughly 90% of the energy input (~ 10^{13} W) into the magnetosphere." The ring current is directly affected by the loss of these particles. The ring current opposes

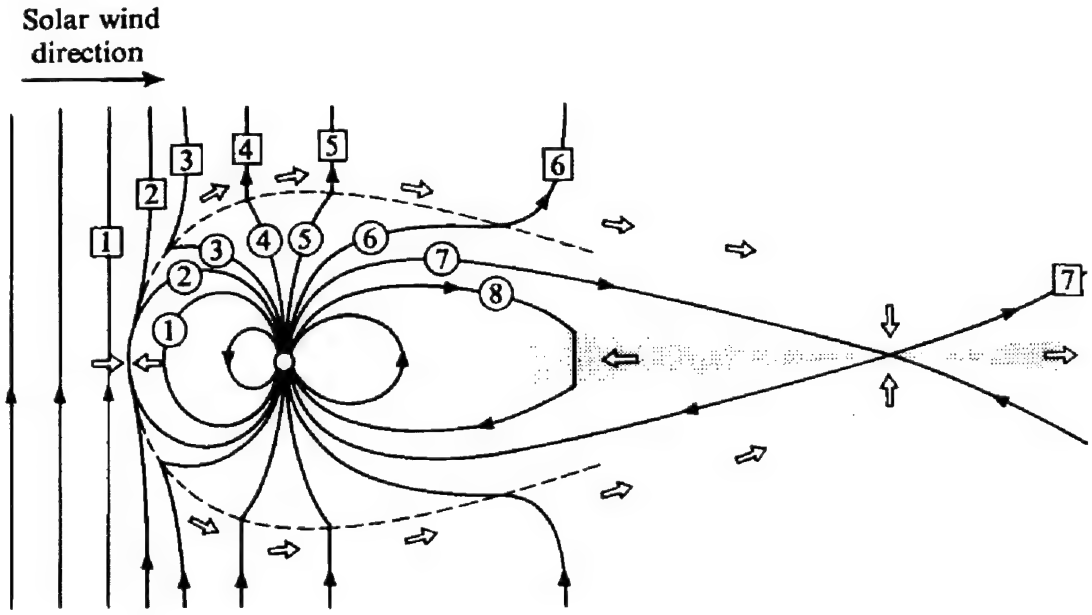

Figure 5. Erosion of magnetic field line in the presence of a southward IMF. (Adopted from Parks [1991:300] from the original proposal of J. Dungey [1961]).

the Earth's magnetic field in the area between the location of the ring current and the Earth and reinforces the Earth's magnetic field exterior to the location of the ring current. In an attempt to reestablish the balance between the ring current and the Earth's field, particles are pulled in from the magnetotail as the Earth's magnetic field lines are eroded. A disturbance created in this fashion is quantified primarily by the geomagnetic index D_{ST} [Baumjohann and Kamide, 1984].

Concurrent with ring current enhancement, another response to increased solar activity begins. As the ionized particles move through the magnetic fields in the magnetotail, small electric fields (~1 $mV \cdot m^{-1}$) are generated [Kelley, 1989:264]. As mentioned earlier, plasma is a good electrical conductor, and so, the magnetic field lines act as equipotential surfaces. As the distance, *ds*, between these surfaces decreases, the electric field increases by

$$\mathrm{E} = -dV/ds \qquad (2)$$

where **E** is the electric field and *dV* is the differential potential. However, as the electric field approaches the ionosphere, the density of ions and neutral particles increases, and the conductivity decreases. The ionized particles contribute to the current density in the auroral region for a short period of time, and increase the auroral electrojet [Kelley, 1991:468]. This disturbance is predominately quantified by the geomagnetic indices AU and AL, which represent the individual strengths of the eastward and westward electrojets, respectively.

Geomagnetic Indices

Geomagnetic indices have a dual purpose: first, to provide information on the geomagnetic activity level when analyzing phenomena linked to it, and second, to study the geomagnetic activity itself and its response to various parameters, from which one can derive information about the magnetospheric machinery.

"The oldest characterization of geomagnetic activity came from the daily estimation of geomagnetic disturbances, but nowadays three families of indices are in use:

(1) D_{ST} index, calculated near the magnetic equator, which describes the ring behavior [Sugiura, 1964]

(2) AU, AL, and AE indices, calculated at auroral latitudes, which gives information on the maxima of the auroral electrojet intensity [Davis et al., 1966]

(3) K indices, which are calculated at all latitudes but are shown to be appropriate mainly at subauroral latitudes; planetary indices are derived from subauroral K indices" [Menvielle and Berthelier, 1991].

From the description above, there are visible differences between D_{ST} and the family of "A*x*" indices. The distinct difference is that the indices measure changes in different geographical locations around the world. The effects which register as changes in D_{ST} occur near the geomagnetic equator, while AE, AL, and AU changes are seen when phenomena occur in the auroral region. The ring current is built from the motion of the trapped energetic particles through the Earth's magnetic field. The auroral electrojets develop due to atmospheric instabilities and particle precipitation from the magnetosphere. They are also influenced by the currents of the magnetotail.

The D_{ST} index has been discussed because of its strong relationship with the solar wind-magnetosphere coupling and its contribution to the K index. It continues to be used in modeling and predicting geomagnetic activity levels, but is of primary importance when related to the effects produced by the ring current.

The auroral electrojet indices AE, AU, and AL were introduced by Davis and Sugiura [1966] as a measure of global electrojet activity and first used by Arnoldy et al. (1970) in a solar wind-magnetosphere coupling study [Baumjohann, 1986]. The AL and AU indices are defined as the negative and positive maxima, respectively, for the variation

of the horizontal component of the Earth's magnetic field (H) in the auroral region [Kelley, 1989:468]. The perturbations are caused by the Joule heating rate of the westward and eastward electrojets, respectively [Perreault and Akasofu, 1978]. The AE index is defined as the separation between the upper and lower envelopes, AE = AU - AL. Since the electrojet currents travel in opposite directions, AE then reflects the value of the total maximum electrojet current.

There are advantages and disadvantages to using the auroral indices (AL, AU, and AE) in solar wind-magnetosphere coupling studies. Since the AE, AL, and AU indices depend on measurements made in high-latitude regions, disturbances taking place in the low-altitude subauroral and equatorial regions do not manifest themselves in these indices. Another disadvantage is that the electrojet may move in relation to the station taking measurements, resulting in a variation being recorded in the absence of a disturbance. These anomalous measurements also take place due to limited number of stations observing the disturbances. AE has an advantage over AL and AU separately since it is only influenced by zonally uniform non-electrojet fields, so movements of the electrojets generally cancel out. Since it monitors the total electrojet current, the AE index is more often used than AL or AU. An advantage in using AL and AU over AE is that one may separately distinguish convection electrojets. The electrojets characterize direct dissipation of solar wind energy and are related to the sudden dissipation of energy previously stored in the magnetotail [Kamide et al., 1985]. AE, AL and AU are advantageous indices to researchers since they are measured at 1 or 2.5 minute time resolution which is much less than the time scale of most substorms and all major storms

(tens of minutes to hours for substorms and several hours to days for major storms). The base value for these indices is the average activity of the 5 internationally quiet days, which is called Sq (averaged solar quiet variations measured) [Berthelier, 1992].

Both the D_{ST} and auroral indices contribute to the creation of the K and a indices. The K and a indices are different representations of the same measurement; a is linearly scaled while K is on a logarithmic scale (Table 2-1). The indices K and a may vary with latitude, longitude, season, or universal time, so a standard for the world has been developed. The Göttingen indices are the recognized world Kp and Ap values (planetary indices), and are published 4 to 5 weeks after their observation. There are 12 worldwide, preselected observing stations (Table 2-2) which record data and report them to Göttingen. They are then corrected to filter out any dependence of the indices other than variations due to the changing solar wind.

Table 2-1. Relationship between Kp and ap. Note: ap is in units of 2 nT, so a measurement of 32 is actually 64 nT. (Menvielle and Berthelier, 1991).

Kp interval	ap, nT	Kp interval	ap, nT	Kp interval	ap, nT	Kp interval	ap, nT
0o to 0+	0	2+ to 3-	9	5- to 5o	39	7o to 7+	132
0+ to 1-	2	3- to 3o	12	5o to 5+	48	7+ to 8-	154
1- to 1o	3	3o to 3+	15	5+ to 6-	56	8- to 8o	179
1o to 1+	4	3+ to 4-	18	6- to 6o	67	8o to 8+	207
1+ to 2-	5	4- to 4o	22	6o to 6+	80	8+ to 9-	236
2- to 2o	6	4o to 4+	27	6+ to 7-	94	9- to 9o	300
2o to 2+	7	4+ to 5-	32	7- to 7o	111	9o to 9+	400

Table 2-2. Magnetic observatories selected for determining Göttingen Ap. (Gehred et al., 1995)

Symbol	Observatory	Geographic		Geomagnetic	
		Lat	Long	Lat	Long
Le	Lewick, Shetland Islands	60 08N	358 49E	+ 62.5	88.6
Lo	Lovo, Sweden	59 21N	17 50E	+ 58.1	105.8
Si	Sitka, Alaska	57 04N	224 40E	+ 60.0	275.4
Rs	Rude Skov, Denmark	55 51N	12 27E	+ 55.8	98.5
Es	Eskdalemuir, Scotland	55 19N	356 48E	+ 58.5	82.9
Me	Meanook, Alberta, Canada	54 37N	246 40E	+ 61.8	301.0
Wn	Wingst, West Germany	53 45N	9 04E	+ 54.5	94.0
Wi	Witteveen, Netherlands	52 49N	6 40E	+ 54.2	91.0
Ha	Hartland, Devon, England	51 00N	355 31E	+ 54.6	79.0
Ag	Agincourt, Ontario, Canada	43 47N	280 44E	+ 55.0	347.0
Fr	Fredericksburg, Virginia	38 12N	282 38E	+ 49.6	349.9
Am	Amberley, New Zealand	43 09S	172 43E	- 47.7	252.5

The Kp and ap indices are measurements of the variation in the horizontal component (ΔH) of the geomagnetic field, filtered and averaged over on 3 hour intervals, which is representative of the time scales of substorms in the subauroral latitudes (1 to 2 hours in duration) [Berthelier, 1992]. The base values are those calculated by a computer algorithm for the solar regular variation S_R, which are the magnetic variations of a geomagnetically quiet day. According to Menvielle et al. [1991], this gives the simplest smooth curve of "K indices-type" variations corresponding to S_R variations.

WIND/SWIM Satellite

The SWIM User's Guide and Reference [Phillips Laboratory, 1995] provides a great deal of information not only about the satellite, but its proposed functions and

capabilities as well. The SWIM (GL-804) portion of the satellite is the primary concern in this research, as these components measure and return the data required. Since its launch in 1994, SWIM has been a proof-of-concept experiment designed to demonstrate space weather forecasting using real-time upstream solar wind data. The satellite remains in a stable trajectory at L1, the point in space on the Earth-Sun line where the gravitational forces balance (~ 240 R_E). The experiments on-board will run at least until NASA's Advanced Composition Explorer (ACE) is launched in late 1997.

Two experiments are of specific interest which will measure constituents and properties of the solar wind and provide the necessary data: the Solar Wind Experiment (SWE) and the Magnetic Field Instrument (MFI). They are explained in the SWIM User's Guide and Reference as: SWE provides the standard plasma parameters of the solar wind: velocity, density, and temperature. MFI provides the three components of the magnetic field of the solar wind (B_X, B_Y, and B_Z) [Phillips Laboratory, 1995:5]. Along with the parameters mentioned above, one simple combination will also be recorded and returned, VB_S, the product of the solar wind bulk speed and the rectified vertical component of the IMF. This index is a hybrid parameter which combines the dynamic and magnetic aspects of the solar wind.

Models

As noted by Clauer [1986], linear prediction filtering (LPF) was originally developed by mathematician Norbert Weiner [1942] for applications dealing with continuous time series. Levinson [1942] adapted this technique to discrete time series,

and his work was included in Wiener's book as an appendix. Magnetospheric researchers have taken advantage of the LPF technique, and have begun to use it, first Arnoldy [1971], as a means of characterizing and predicting geomagnetic activity using solar wind data.

The use of LPF is restricted by two basic assumptions. The first assumption is that the data is stationary. Stationarity indicates that the statistical properties of the input and output do not change with time [Makridakis and Wheelwright, 1978:263]. A criterion to establish that the data is stationary has been developed. Examination of the autocorrelations of the data will indicate 95% of the coefficients lie within a range of plus or minus 1.96 standard deviations from the mean of the autocorrelations. The second assumption is the input and output are related by a linear relationship. If they are not related by a linear relationship, LPF results are erroneous since the explicit purpose of using LPF is to return a linear filter. Therefore, linearity and stationarity have been considered pertinent assumptions for this data set.

Three authors' works are of historical interest and important to the undertaking of this thesis. Bargatze et al. [1985], Clauer [1986], and Vassiliadis et al. [1995] have written papers which detail the use of LPF with respect to the problem of solar wind-magnetosphere coupling. Bargatze et al. [1985] assembled a data set, and established the magnetospheric impulse response using moving-average linear filter analysis. Clauer [1986] used the Bargatze data set to show the applications of LPF in magnetospheric studies with different geomagnetic indices and input time series. Vassiliadis et al. [1995] advanced this research by introducing the use of a state-input space method using

nonlinear equations of state for the magnetosphere. Vassiliadis furthered improved his attempts by working with multiple input time series in his analysis. Although he did not use LPF, he broadened the approach to modeling geomagnetic activity by using multiple inputs to capture greater detail of the interactions taking place.

LPF uses a filter to model the most general, linear relationship between the measured magnetospheric and solar wind quantities as shown below [Bargatze, 1985:6387]:

$$O_T = \int_0^{\infty} H_\tau \cdot I_{T-\tau} \, d\tau \qquad (3)$$

In this continuous time model, H_τ is the filter, O_T is the output parameter, $I_{T-\tau}$ is the input parameter at time $T-\tau$, T is the time of the observation, and τ is the time lag. The variable names O_T, H_τ, and $I_{T-\tau}$, scalars for single input-output models, will remain the same for all of the models demonstrated. That is, even for multiple input models, the input variable will remain $I_{T-\tau}$, even though it will have several components. To use this model for multiple inputs or outputs, substitution of matrices must be made for the scalars.

Using Equation [3], the geomagnetic index AL, output, can be predicted once the filter H has been determined. For given input(s) of the solar wind coupling functions, LPF constructs the filter H_τ by minimizing the least-square errors associated with estimated and observed outputs. Although the integral in Equation [3] extends to infinity, practical applications use a predetermined number of coefficients which model the effects of the input reasonably. These coefficients correspond to the time lags which have a significant impact on the calculation of the output O_T.

Bargatze et al. [1985] and Clauer [1986] used the magnetic index AL as the output parameter (O_T) and the solar wind parameter VB_S (the product of the solar wind bulk speed and the rectified B_Z component of the IMF) as the input ($I_{T-\tau}$) for the LPF model below. Clauer [1986] extended this research to include other outputs to be tested using similar coupling functions as inputs over discrete time intervals. Equation [3] then becomes

$$O_T = \sum_{\tau=0}^{\infty} H_\tau \cdot I_{T-\tau} \qquad \textbf{(4)}$$

The only difference between the continuous and discrete models is the form of the equations being solved under least squares error techniques. For Equation [3], the equations are integrals while for Equation [4] the equations contain summations. Single channel (single input-single output) and multichannel filters (multiple input-single output) were used to predict AL in this thesis while Clauer used only single channel models.

Clauer [1986] made use of several parameters as input: VB_S, V^2B_S, and $VB_T^2\sin^4(\theta/2)$. The first is the same parameter used by Bargatze [1985], the second was introduced by Murayama and Hakamada [1975], and the third was initially used by Perreault and Akasofu in 1978. The coupling function inputs used in solar-wind magnetosphere studies fall into three major categories: (1) simple expressions, (2) electric field-related, and (3) power-related. VB_S is the rectified solar wind convective electric field developed by Rostoker et al. [1972]. V^2B_S is considered a simple coupling expression, i.e., just a relationship between two components of the solar wind. $VB_T^2\sin^4(\theta/2)$, called the epsilon parameter, ε, is a coupling function relating the power in

the solar wind to geomagnetic activity. These functions are the actual inputs, I, to the LPF model.

Vassiliadis et al. [1995], employing a state-input space formalism rather than LPF, used the same input parameters as Clauer [1986]. State-input space models are a pattern-recognition technique which classifies activity "patterns" in time series data by associating them with points in the space vector [I O], where I and O are the input and output vector spaces, respectively. The space vector is a multi-dimensional vector whose points represent a magnetospheric-solar wind event. The input is related to a reference point of the output space vector by its magnitude and orientation. A predefined distance is set about the reference point, and any "neighbors", output points from similar inputs, are used to determine what the output values corresponding to the new input will return [Vassiliadis et al., 1995].

Vassiliadis et al. [1995] discusses the comparisons between linear filters and their predictive capabilities and those using nonlinear techniques. The values of the correlations provided by Vassiliadis and Clauer will be used in the verification and comparison of the linear filters' predictions.

Verification

The primary means of verification will be to use correlations between the measured AL index and the predicted AL returned by the models. The prediction-observation correlation relationship, used by Vassiliadis [1995], establishes the correlation between a predicted and observed time series over some interval of time. Least squares error

minimization of the time series is inherent in the LPF technique, and adds an additional support in achieving the optimal models.

LPF is based on minimizing the least squares error of the time series, and producing the most general linear filters (functions which transform the input into the output) possible. In determining the filter coefficients by this criterion, one must minimize the error between the different time series by subtracting the actual or measured output from the computed or predicted output [Clauer, 1986:41].

The prediction-observation correlation relationship is defined as

$$C_{AL} = \frac{\frac{1}{T} \cdot \sum_{i=1}^{T} (AL_{t+i} - |AL|) \cdot (\hat{AL}_{t+i} - |\hat{AL}|)}{\sigma_{AL} \cdot \sigma_{\hat{AL}}} \qquad \textbf{(5)}$$

where C_{AL} represents the correlation value between the observed and predicted time series over a given time interval T, T is the time interval over which the series is viewed, i is the time increment, AL is the value of the observed index AL, $\hat{AL}$ is the value of the predicted index, and σ_{AL} and $\sigma_{\hat{AL}}$ are the standard deviations of the observed and predicted AL indices, respectively.

The predicted values of AL will be correlated with the measured values of AL to determine the accuracy at which the models performed. Previous works [Bargatze, 1985; Clauer, 1986; Vassiliadis, 1995] have used this method to compare the results of single input LPF and state-input space methods with measured values. Vassiliadis [1995:3503] reports the average correlations between predicted and measured values of AL to lie between 0.50 and 0.65.

III. Methodology

In this chapter, the methodology and approach to predicting the AL index will be presented in seven sections. The first section will describe the coordinate system in which the measurements of the solar wind data were made. The second section will show the identification and construction of the coupling functions which will be used as inputs to the models. The third section will discuss the terminology used with the models, the types of models which can be used, and how each type of model approaches prediction. Section four establishes the procedure for construction of the models used for predicting AL in this research. The fifth section will explain the approaches to prediction, the prediction requirements, and the comparisons of the model outputs with persistance. The sixth and seventh sections will describe the use of the impulse and frequency response functions as tools for the analysis of the model's output and filter coefficients.

Reference Coordinate System

The Bargatze data set provides raw data from the WIND/SWIM satellite in GSM coordinates. The GSM coordinate system is a right-handed Cartesian system with its origin at the center of the Earth [Figure 6]. The positive x axis is directed toward the Sun, and the z axis lies in the plane containing both the x axis and the geomagnetic dipole axis. With these conditions established, the y axis can not lay in the ecliptic plane at all times. Therefore, the z axis will oscillate with the geomagnetic coordinates (through 23 degrees) as the geomagnetic dipole axis rotates over a period of one day. GSM coordinates are

useful to reference data from the distant magnetosphere since the whole magnetosphere is expected to shift position, to a first approximation, as the dipole axis moves [Handbook of Geophysics, 1985:4-3]. Additional details concerning the data set can be found in the Scope and Limitations section of Chapter I.

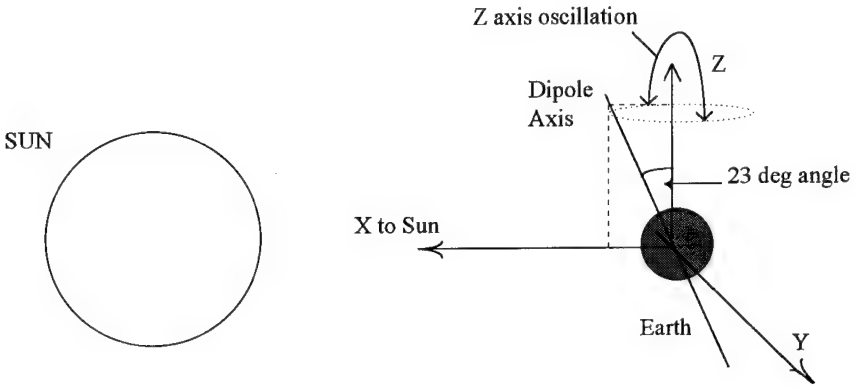

Figure 6. The Geocentric Solar-Magnetospheric (GSM) Coordinate System.

Identification and Construction of Model Inputs

Bargatze has ordered the data set into 34 intervals of increasing geomagnetic activity, moving from low activity (quiet) through moderate to strong activity (geomagnetic storm levels). Appendix A reveals the data format and units for all of the data to be used in this study. The beginning and ending points of each interval are identified in Appendix B as well as the number of hours spanned by each interval, number of data entries, and the input parameters to be used, averaged for each interval.

In order to model the geomagnetic activity, the original data must be transformed and built into coupling functions, or inputs. Coupling functions are parameters whose values are in some way related to an observed or predicted phenomenon. The construction of these coupling functions requires some alteration and assembly of the original data parameters. The B_Z component of the IMF is rectified and identified as B-South, B_S, where :

$$B_S = \begin{cases} 0, & for\ B_Z \geq 0 \\ -B_Z, & for\ B_Z < 0. \end{cases} \quad \textbf{(6)}$$

This southward component of the IMF is utilized to help form 2 of the 3 inputs which are used by LPF techniques, namely B_S and VB_S.

A second parameter, highly correlated with the geomagnetic activity, is the power of the solar wind incident on the magnetosphere [Gonzalez, 1990]. This quantity, $\varepsilon = VB_T^2 \sin^4(\theta/2)$, is constructed from the data set according to the following procedures:

$$\theta = \begin{cases} \tan^{-1}\dfrac{|B_Y|}{|B_Z|}, & for\ B_Z > 0 \\ \pi - \tan^{-1}\dfrac{|B_Y|}{|B_Z|}, & for\ B_Z < 0 \end{cases} \quad \textbf{(7)}$$

$$B_T = \sqrt{(B_X)^2 + (B_Y)^2 + (B_Z)^2} \quad \textbf{(8)}$$

where B_X, B_Y, and B_Z are the components of the IMF, θ is the angle at which the IMF interacts with the magnetosphere, and B_T is the total IMF strength.

Model Terminology

This thesis investigated autoregressive (AR), moving-average (MA), and autoregressive moving average (ARMA) models used in representing and predicting time series data [Makridakis and Wheelwright, 1978:252-309]. An AR model uses a linear combination of past output values to compute a new value for the output. The general equation form which represents all three different model types is given by:

$$a_1 \cdot O(t) + a_2 \cdot O(t-1) + \ldots a_{\tau+1} \cdot O(t-\tau) = b_0 \cdot I(t) + b_1 \cdot I(t-1) + \ldots b_\tau \cdot I(t-\tau) \quad (9)$$

where O is the output time series, I represents the input time series, and a and b are the coefficients which are computed through least square error minimization using LPF. When using multiple inputs to the LPF models, each of the inputs will have a separate series of b coefficients and I inputs while there will be only one set of a coefficients for any model.

For AR models, the only input variable is an earlier output value, so the term auto is applicable, while regressive refers to going back along its own timeline. Using least squares minimization, coefficients for these earlier values are determined and used to calculate the new output. MA models use linear combinations of the past errors between

actual and predicted output values with computed coefficients to influence the importance of each error. The predicted output values mentioned above are actually the calculated values of the output at time t. The AR and MA models are considered to be special cases of a more general model. An ARMA model uses linear combinations of both the past values and past errors to achieve the new output [Makridakis and Wheelwright, 1978].

An important feature of each of the types of models is that they have the ability to increase their order. The order of a model identifies the number of earlier values entering the linear equation relating "output" to "input". For example, an AR model of order 2 includes the current value and the previous 2 values of the output variable. Likewise, an MA model of order 2 uses the current error and the previous 2 errors between the predicted and actual output. An ARMA model which combines these two models would be classified as ARMA(2,2).

As the models increase in order, successively larger numbers of previous errors or values will be required for the model to begin optimizing the filter coefficients. For large time series, this poses a small problem since a great deal of prior data can be used to optimize the filter before real-time analysis is required. For small time series, however, this is a significant problem. If there are an insufficient number of data points to allow optimization of the filter coefficients, initial estimates must be made so that the filters approach the ideal values more quickly. This can be done by solving a system of nonlinear simultaneous equations of n dimension, where n is the order number. A detailed description of the procedure to develop the system of equations can be found in the

mathematical supplement appendix of chapter 9 of Interactive Forecasting: Univariate and Multivariate Methods [Makridakis and Wheelwright, 1978].

The input variables need not begin with the current time. In many circumstances, a delay is introduced. A delay indicates the value, measured in time intervals, of the temporal offset or lag. For example, a delay of 4 would mean the input for an AR, MA, or ARMA model would begin with the 4th previous value or error as the current value or error. If the order was 2 for the AR or MA models, the fourth, fifth, and sixth previous values or errors would be used to determine the next output. For ARMA, the same previous values and errors would be used in the models together. In all of these cases, associated with the values and errors is a set of coefficients which determine how they influence the new output.

The representation for a second order AR or MA model with a time delay of 4 used to compute the next value of an output is, therefore, given by:

$$a_1 \cdot O(t) = b_0 \cdot I(t-4) + b_1 \cdot I(t-5) + b_2 \cdot I(t-6) \qquad \textbf{(10)}$$

where O is the output, I are the past values of the outputs or errors of the AR or MA models, respectively, used as inputs and a_i and b_i are the coefficients to be used in construction of the filter for this model. The equation for an ARMA model would be very similar, the only difference being the right hand side of Equation [10] would contain an additional, similar set of terms. One set of inputs and coefficients would pertain to the past values of input and the other to past errors.

The coefficients in Equation [9] and [10] are the filter coefficients or amplitudes. The filter is built by selecting a specific model, delay, and order for the data set. On a point-by-point basis, the filter coefficients would change continually throughout a data set. By minimization of the least-squares errors, partial derivatives of Equation [10] with respect to the coefficients are computed, and the filter coefficients are optimized over a given time interval. This optimization technique, the foundation for adaptive filtering processes, provides the best fit for linear methods over the whole data set.

The construction and analysis of the models was performed using a suite of procedures in the Matlab® System Identification Toolbox®. The ARX function is given the input-output (IO) data, in the form of coupling functions, the order of the AR model to use on the input and output, and the time delay and computes the loss function for each model [Ljung, 1992]. The loss functions for each different model were calculated using the ARXSTRUC command. This command computes the loss function of each model by a cross validation technique, also known as Akaike's Final Prediction Error (FPE) criterion. The loss function over a desired interval is the difference between the actual output value and the predicted value generated by the model's least-squares error estimate. The loss functions were then sorted, by the SELSTRUC command, to find the smallest FPE, which is given by

$$FPE = \frac{1 + n / N}{1 - n / N} * V \qquad \textbf{(11)}$$

where n is the total number of estimated parameters, N is the length of the data record, and V is the loss function for the structure in question [Ljung, 1992].

There are several types of loss functions which can be computed depending on the size of the data set or how the data set is used in the model. For small data sets or where the interval to be tested includes all of the data points, a different method of computing the least squared errors is suggested. Using the Matlab® software, there are at least two alternatives to using Akaike's FPE method. They are Akaike's Information Theoretic Criterion (AIC) and Rissanen's Minimum Description Length criterion (MDL) [Ljung, 1992:1-52-3]. They are given by:

$$AIC \approx \log\left[(1+\frac{2 \cdot n}{N}) * V \right] \tag{12}$$

$$MDL = \left[1+\log(N) \cdot \frac{n}{N} \right] * V \tag{13}$$

respectively. The variables used in Equations [12] and [13] are the same as those used in Equation [11].

Model Construction

The construction of the models to predict the AL index consists of several steps. The first step involves the testing of the coupling functions or inputs to determine if they are going to provide good correlations. If the coupling functions are not related to the output at all, there is no reason to build the models containing them. Secondly, the models are built using the coupling functions and the measured AL values using LPF

techniques. Finally, the models' outputs, the predicted AL for each model, are compared by correlating the measured and predicted AL values.

The measured AL and coupling function values are correlated to determine the prudence of using the coupling function as an input to a model. Matlab® computes the cross correlations between the inputs and the measured values of AL using the CORRCOEF command. CORRCOEF uses the covariances of the input and output matrices to compute the correlation coefficients matrix by Equation [14], where

$$Corrcoef = \frac{C(i,j)}{\sqrt{(C(i,i) * C(j,j)}} \tag{14}$$

and C is the covariance matrix for the input(s) and output and (i,j) indicate the respective covariance elements. If the input(s) correlated perfectly with the AL index, the correlation values would equal unity, indicating input(s) and output amplitudes and phases are coincident. The proximity of the correlation values to unity indicates the accuracy of fit between the input(s) and the output.

Once the inputs have been tested to insure they will provide good results, the coupling functions can be entered into the model. The filter coefficients were created using the ARX command, which performs AR techniques of order X to return the least-squares estimate of the filter coefficients for each model. Models were constructed in groups of several thousands at a time, encompassing orders from ARMA(1,1) to ARMA(150,200) with time lags extending from 0 to 250 time steps, or real-time lags of 0 to 10.5 hours.

The filter coefficients which were generated by the models were saved and used to predict values of the AL index. The input(s) and filters were used by the IDSIM

command to predict the output values of AL. IDSIM uses a built-in FILTER function to implement a standard difference equation and solve for the output values [Matlab, 1992]. The difference equation uses all of the filter coefficients and time delays recorded in a model to produce the simulated output using the input matrices (one or more) being investigated. The loss functions, discussed above, were then computed to find the optimal set of filter coefficients for each coupling function.

Once the output has been generated, Equation [14] is again used to determine how well the model has performed by calculating the correlation matrix between the predicted and measured values of AL. Typical values for the correlation have averaged from 0.50 to 0.65 in previous studies, depending on the coupling functions used as input [Vassiliadis, 1995:3503]. This correlation describes the ability of the model to predict the AL index given the same input values over the same period of time. The correlation values achieved using single and multiple inputs for these models will be discussed in Chapter IV and the actual values can be seen in tabular format in Appendix D.

Prediction

The prediction of geomagnetic activity has a large number of possible users in both the military and industry. Most users would request an 8 - 12 hour forecast of geomagnetic activity to enable them to terminate current operations and protect assets, or to allow time to redirect operations to alternative methods. Currently, such long range predictions are based on the use of persistance and a forecaster's discretion. Although

these methods are currently accepted as the most reliable, a computer model with a guaranteed level of reliability over this period of time would gain acceptance very quickly.

The models used in this research are capable of making forecasts nearly this far into the future. This capability is directly related to the location of the satellite recording the solar wind parameters and the model's ability to predict AL several time steps into the future. The data which is received by the WIND/SWIM satellite will precede the arrival of the physical components of the solar wind at the magnetopause by approximately 45 minutes. However, for high solar wind speeds, this time may be more than halved. In addition to this lead time, the solar wind requires, theoretically, at least one hour to interact with the magnetosphere. This provides input to the models, once the data are incorporated into coupling functions, nearly 2 hours prior to any expected increase in geomagnetic activity. By combining the time delays inherent in the data and short term predictions, of approximately 2.5 hours, by a model, a total forecast time of 3.5 to 4.5 hours can be achieved. Thus, a more detailed forecast in terms of both onset time and magnitude of expected geomagnetic activity is achievable.

In order for the models to make these predictions correctly, two major prerequisites must be fulfilled. The first requirement is that there must be input data for the model to run and there cannot be gaps in the data set. If there are gaps in the data or no data at all, the model cannot run without incorporating interpolation or substitution. From Equations [3] or [4], the model needs both an input and the predetermined filter coefficients in order to predict the output. The second major requirement is that the input data must be measured on the same time scale as the data which was used to develop the

filter coefficients. If this requirement is not fulfilled, the predicted AL values will not be comparable with the measured AL values.

The different types of prediction which can be performed with completed models are the single-step and the block forecast methods. The first method, the single-step method, predicts each step out to the time desired. By using each predicted value of AL as an actual value of AL, the single-step method propagates until it has reached the desired prediction time. The single-step method of prediction should not allow any significant errors to occur as each value of AL is generated using actual values of the solar wind input and a proven filter.

The second method, block method, uses past data, propagates it forward in time, and reuses it as a new set of input data. Even if the solar wind parameters change radically over a time period of half an hour, this method can produce reasonable results. This effect can be explained by considering the impulse response of the system. The "peaks" of the impulse response show that the system can "remember" inputs for approximately 90 minutes. Therefore, small blocks of past input data can be replicated and brought forward in time to keep a model running without severe effects on the output.

The main detriments to this method are that the values of the output, AL, are not known ahead of time, and if there are significant variations in the solar wind data, the model will under- or overpredict the actual values of AL, dependent on the characteristics of the data which are made use of in the forecast. If the data used in the forecast contains solar wind parameters which produce strong geomagnetic activity, the model will forecast

extended periods of strong geomagnetic activity when, actually, the activity may decrease as the solar wind components drop in intensity.

The lack of input data is the primary restriction of the models to forecasting out to tens of hours or days. Forecasts made using persistance can be used for general activity levels of geomagnetic activity, but do not provide specific onset times or specific levels of activity. Generalized forecasts can be made by recording the positions of long lasting disturbances and features on the Sun, and predicting their return. By measuring the intensity of the disturbances on the Sun and the geomagnetic activity level they generated, a relationship can be developed to predict average activity levels on a monthly time scale. This method is not useful to organizations which must continue or can only shut down operations for short periods of time.

Persistance, on the other hand, takes the measure of the previous time period's activity level and uses it to predict the value of the next time period's activity level. Obviously, this method does not consider any changes in the solar wind parameters over a given interval. As such, it will be unable to predict sudden increases or decreases in the geomagnetic activity levels. Since there are eight time periods in each day for predictions, this method may also predict unreasonably high or low levels of activity. Again, this method should not be forwarded to users since it does not consider changes which may take place in the solar wind and, therefore, in the geomagnetic activity.

Impulse Response

The impulse response is the magnitude of the output at time τ resulting from an input of unity at time $\tau = 0$. The filter coefficients which were generated by the LPF techniques are used to transform a single value of unity input into the AL output values over the time interval the filter covers. As described in coordination with Equation [4], the filter is of finite length, covering the time lags which are most important to approximate the actual output with the predicted values.

The impulse response curves shown in Figures 7a and 7b were built with a constructed input time series, the predetermined filters, and the IDSIM command from Matlab® which uses the filters to transform the input into the output. The time series input consisted of an hour of zero input, a single input of unity, and followed by a time series of zero inputs. The initial zero input values were to ensure the filter was stable and responded only to non-zero inputs. The single value of unity allows the filter to respond to a unit input at each individual time lag. The response from the filter shows the impulse response of the output. Since the input value is unity and only zeroes follow it in the time series, the impulse response is also the magnitude of the individual filter coefficients. The zeroes trailing the single unit input allow the filter to show how the individual coefficients transform the normal time series input into the predicted index AL.

In order for the exact relationship between an input and an output to be shown, the impulse response curve must be finite in length. A perfect curve would go to zero and remain there after all of the coefficients contributing to the output were used. The "memory" of the impulse response would "recall" the events that have taken place earlier

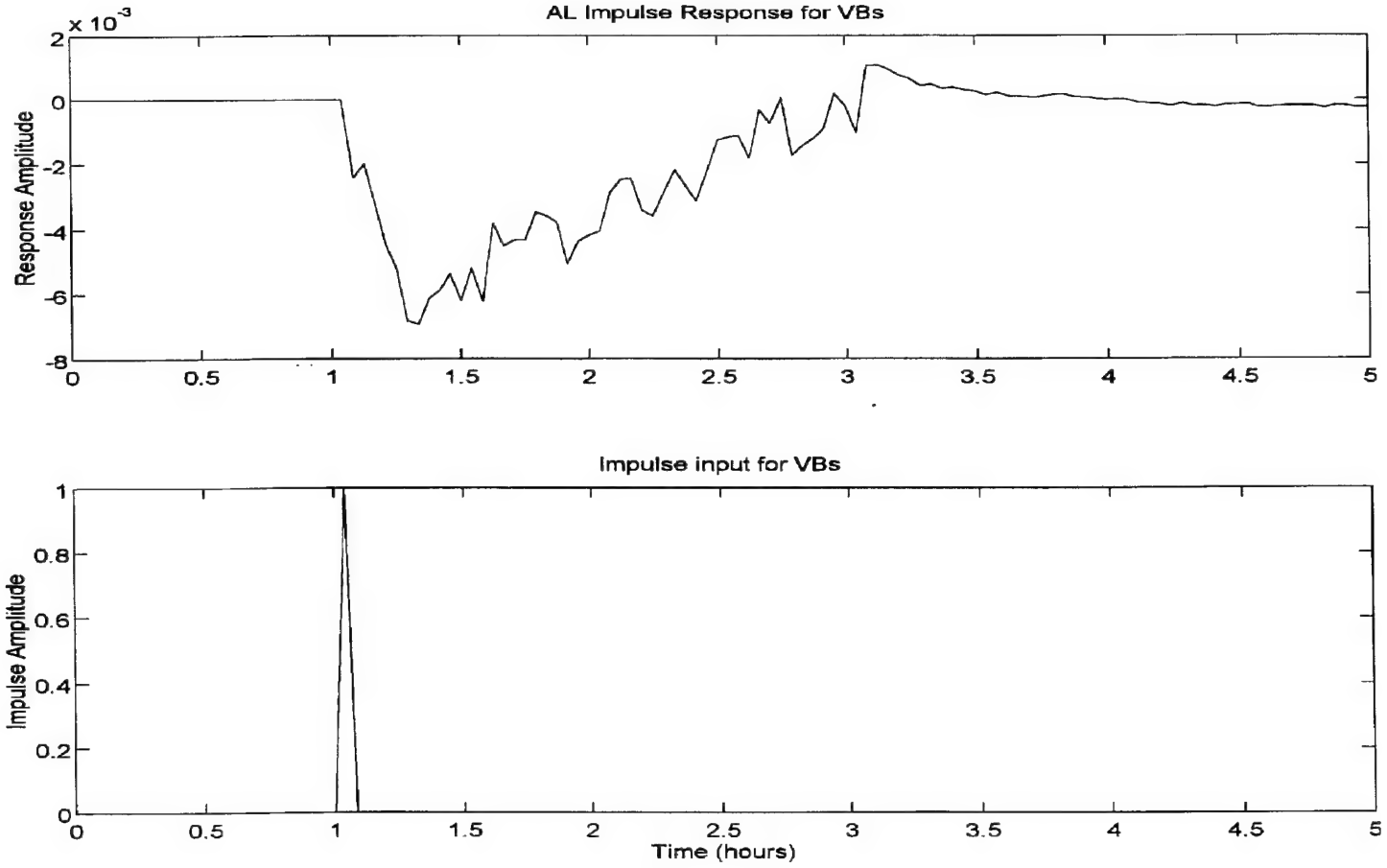

Figure 7a. Impulse response curve for VBs.

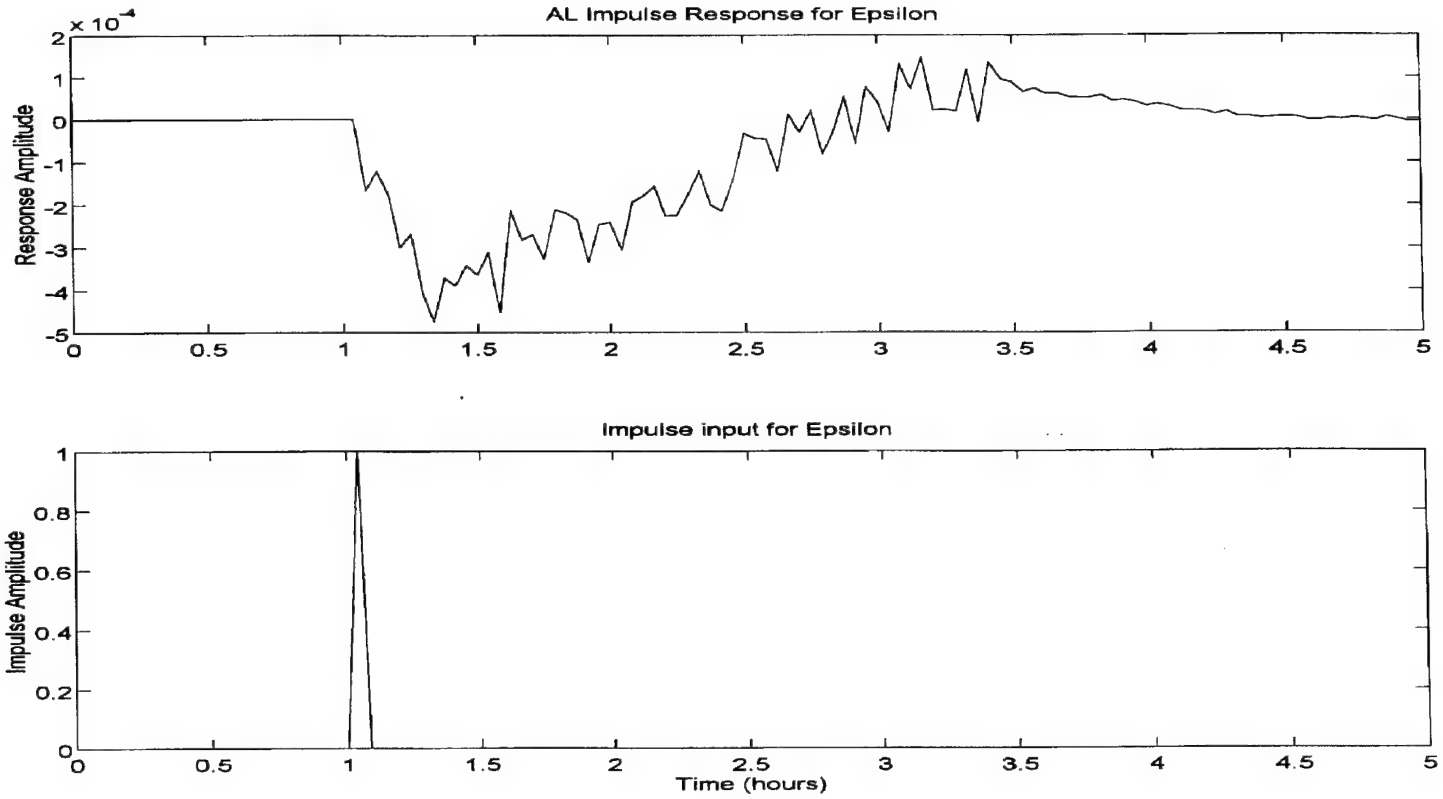

Figure 7b. Impulse response curve for epsilon.

and use these coefficients until the physical system "forgot" the event had occurred. In other words, the original event would have moved into the past far enough that the impulse response no longer viewed it as a contribution to the current state of geomagnetic activity. The system memory would then represent energy input, energy storage, and eventually, energy dissipation.

Figures 8a and 8b show the impulse response curves for the convective electric field coupling function, VB_S, over moderate and strong geomagnetic activity regions (intervals 10 to 14 for moderate and 27 to 31 for strong). These intervals and activity levels chosen because they represent a wide range of possible solar wind inputs to the models. They were also used in previous studies [Clauer, 1986] and could be compared to them for accuracy and validation. The curves were created through correlation and covariance analysis methods using the Matlab®'s CRA command. The cross correlation values are an unscaled measure of the impulse response. Properly scaled, these values return the impulse response curves for the different inputs.

The structured curves in each figure represent the actual filter coefficients for the given time intervals or geomagnetic activity levels. The smooth curves in Figures 8a and 8b are presented as general guides to locate general peaks and minimums. These curves help to indicate which time lags in the filter are most important to correctly predicting the output.

By examining these curves, the importance of past values of the input becomes clear. The curves in figure 8a show two predominant peaks at approximately 12 and 30 time lags, or 30 and 75 minutes, respectively, for moderate geomagnetic activity. The

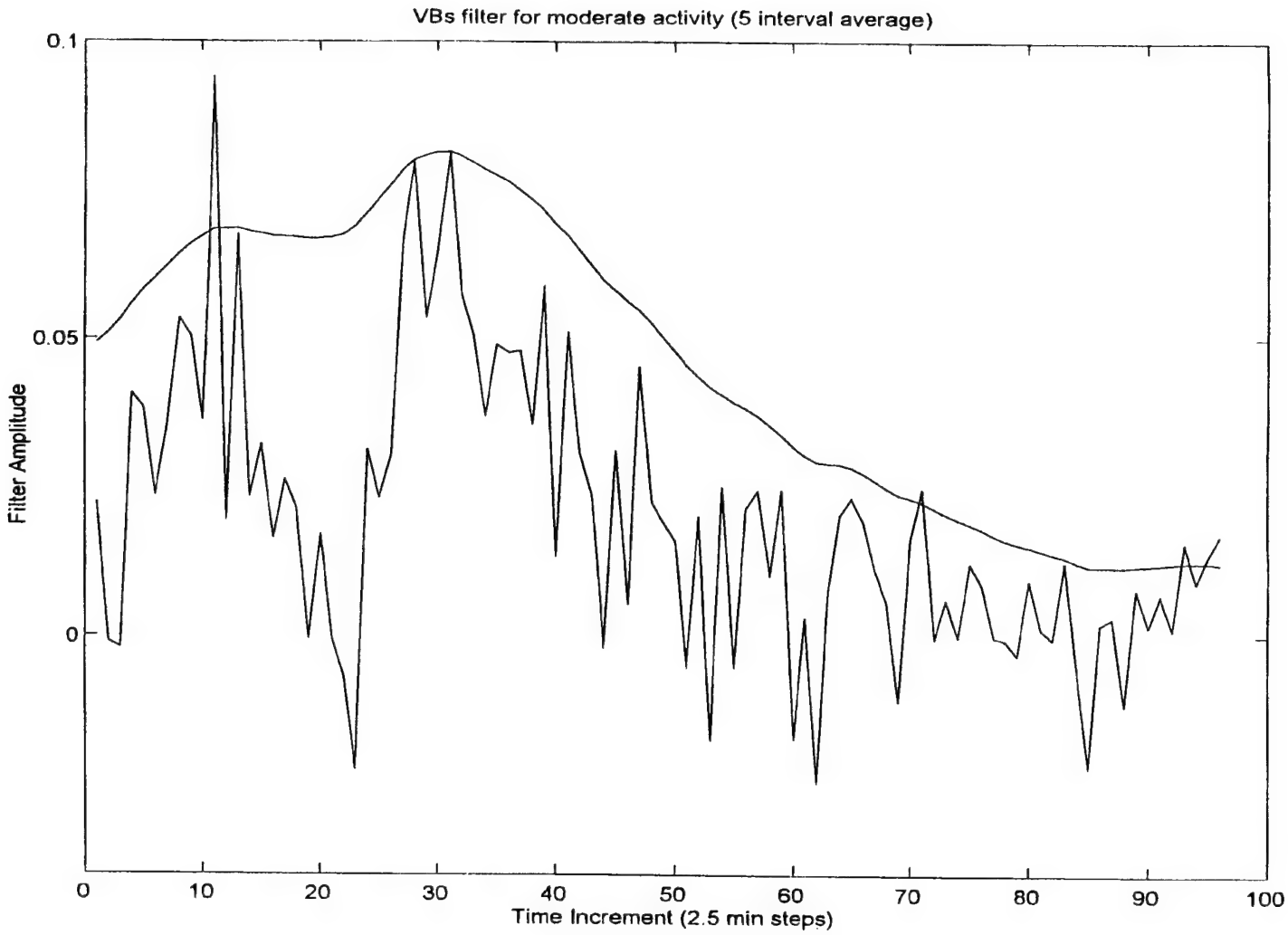

Figure 8a. Impulse Response Curve for VBs in moderate geomagnetic activity.

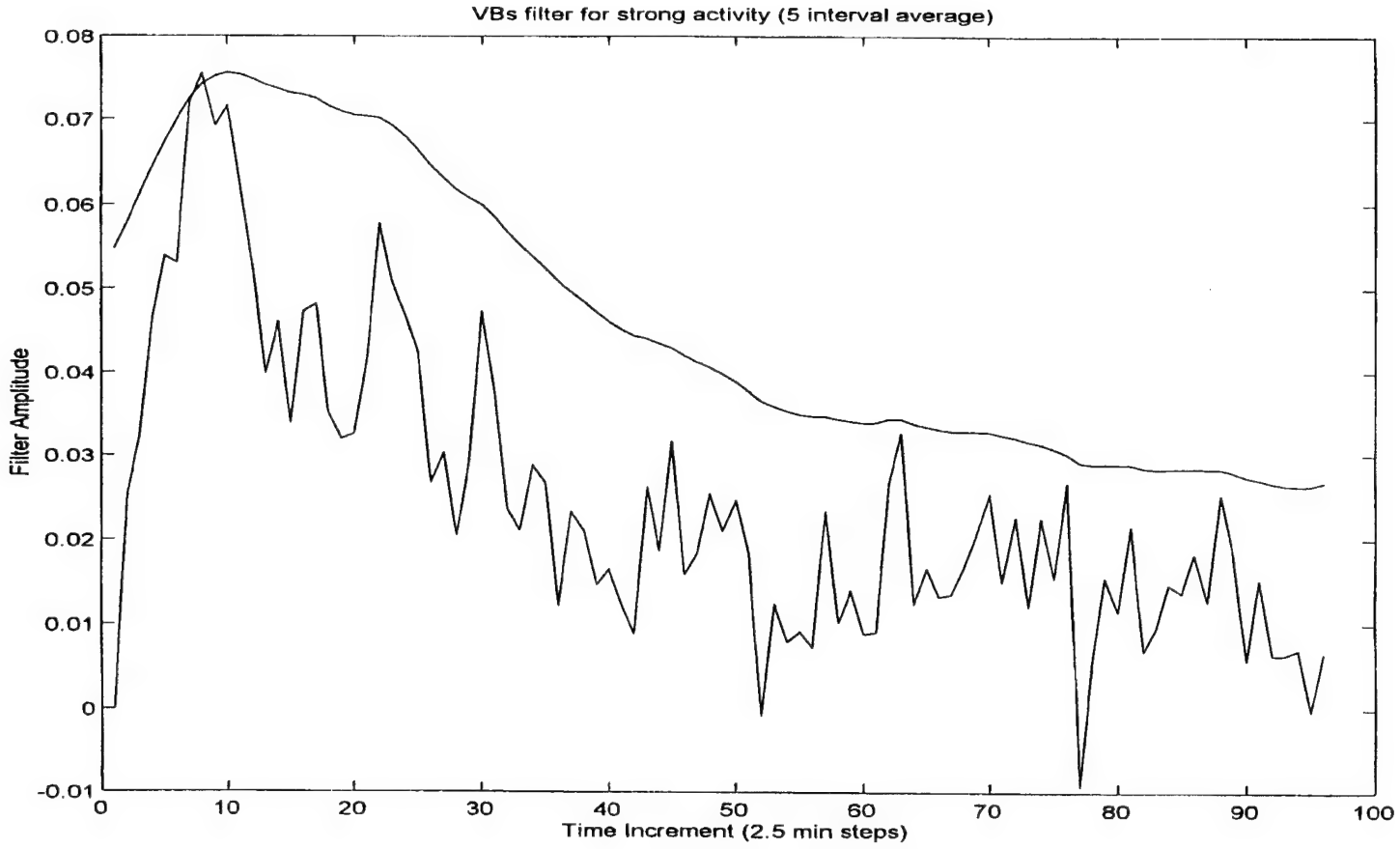

Figure8b. Impulse Response Curve for VBs in strong geomagnetic activity.

rest of the curve decays gradually to near zero values. The curves in figure 8b shows a single general peak at approximately 10 time lags, or 25 minutes after which the curve decays towards an amplitude of zero. The peaks in both figures relate the importance of events at these earlier to the current values of the output, AL. Analysis of the mechanisms behind the peaks will take place in Chapter IV.

These curves helped to develop the models used to predict the magnetic index AL and compare it to the measured AL in the Bargatze data set. The models were initially built using the software's default filter length (20 coefficients). Once the new corresponding impulse responses were viewed, the filters were determined to be far too short in length to estimate the model properly. At this point in the analysis, the models were rebuilt several times until their impulse response curves showed that the magnitude of the filter coefficients decayed to and remained near values of zero. The drop in the amplitudes of the impulse response indicated that the current filter length was sufficient to model the greatest portions of the variability in the output. Any further increase in the filter length would not benefit the predictive quality of the model significantly, and would increase the computation time of the model to where the model itself would no longer be useful.

Frequency Response

The frequency response is a time domain description of the predictive model. This is important because the predicted and measured outputs must correlate well at frequencies corresponding to geomagnetic storms and substorms in order to model

geomagnetic activity. Geomagnetic storms and substorms occur on frequency scales of $1 \cdot 10^{-4}$ and lower and $6 \cdot 10^{-4}$ to $1 \cdot 10^{-4}$ $^{rad}/_{sec}$, respectively. If the model can account for changes in frequency phase and amplitude in the ranges of storms and substorms, it should predict geomagnetic activity well. The higher frequency scales correspond to individual data measurements, on the order of $7 \cdot 10^{-3}$ $^{rad}/_{sec}$ and above. If the predicted frequencies match the phase and amplitude of the measured AL index, the model should be able to predict the output well from step to step.

The AL frequency response derived from a single input, VB_S, prediction is compared with the actual AL outputs in Figure 9. The upper plot in Figure 9 is the amplitude comparison of the actual and estimated data while the lower plot is the phase comparison. The frequency phase responses of the two models correspond well in the lower frequency regions, indicating that the predictive model should do well in predicting onset and duration of the geomagnetic activity at storm and substorm levels. The frequency amplitude responses are of the same order of magnitude for the lower frequencies so we should expect that the predictive model will tend to deviate from the actual intensity of the geomagnetic activity by a small amount.

As the frequency response function moves into the higher frequency regions (moving to the right), the phase responses diverge. This would indicate that the model will not respond closely with the actual AL index for each time step. However, since the general shape and trend of the curve remain similar to the actual phase, the model will not become erratic and unstable. The amplitude response of the model remains very close to the actual amplitude responses of AL. The amplitudes of the model's responses should,

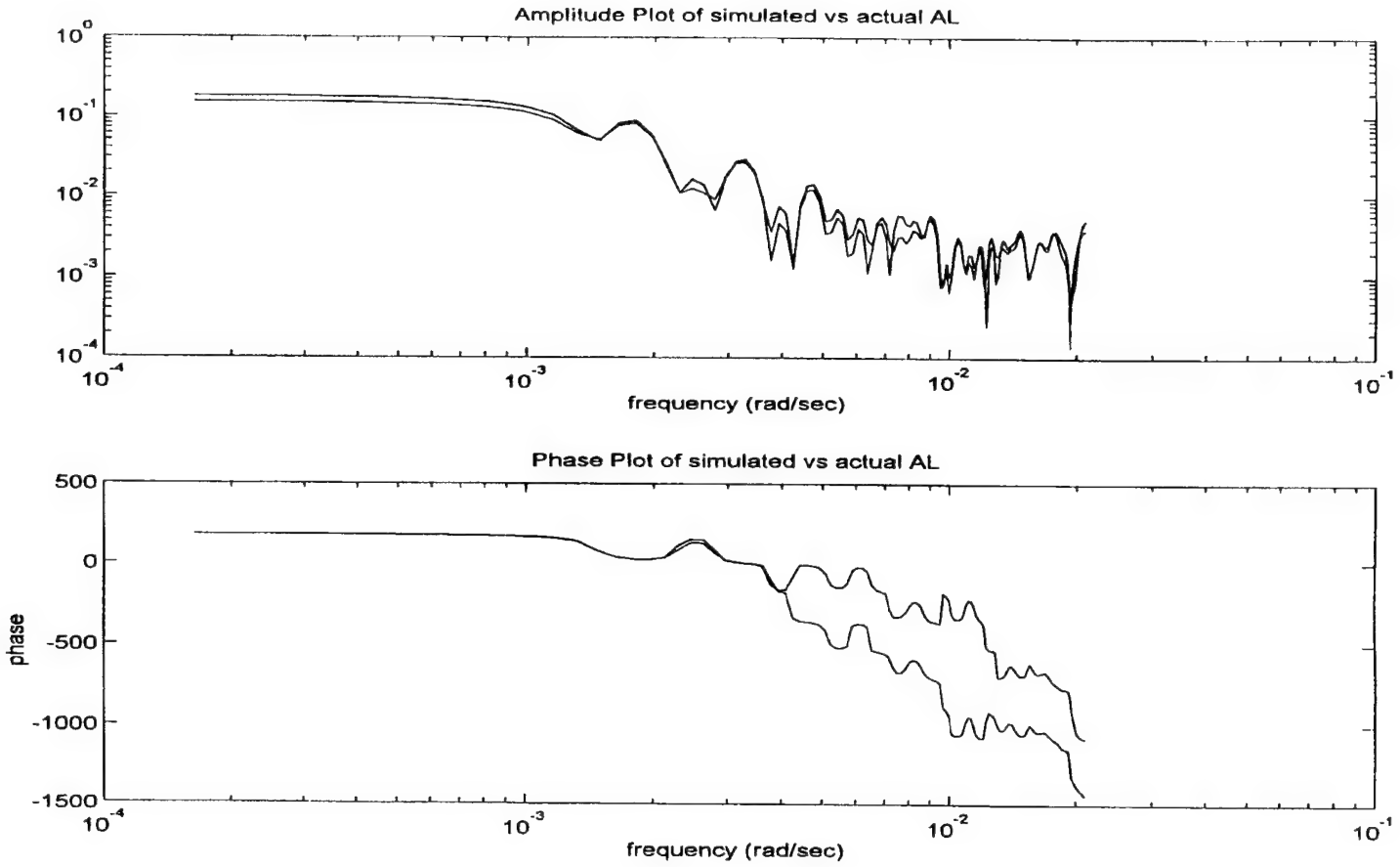

Figure 9. Frequency Response of actual and simulated AL.

therefore, remain relatively close to those of the measured AL regardless of the frequency. The errors in the simulated model will be apparent primarily by small deviations in amplitude throughout the frequency range of inputs and by the model's inability to respond exactly as the actual AL index does for the individual inputs.

The present analysis of the model frequency analysis confirms in the works of Bargatze [1985]. He concluded that although the VB_S and AL time series contain a high-frequency component, the high-frequency components are not correlated. This would indicate the magnetosphere acts as a low-pass filter for the solar wind variations [Bargatze et al., 1985]. Since the correlations for the multiple, and even single, input models in high, the high frequency components of the time series do not add significantly to the correlation of the models.

IV. Results and Analysis

In this chapter, the results obtained from this research will be examined and compared with the results reported by Bargatze et al. [1985], Clauer [1986], and Vassiliadis et al. [1995]. The information will move in a logical fashion from the basic theory and parameters through the actual analysis to the attempts at forecasting. The next four sections will discuss comparisons of the impulse response curves, filter and model content, the residuals and correlations for the different models, and the forecasting results.

Impulse Response

Bargatze's paper describes the development of a series of filters based on the geomagnetic activity level. The filters are actually just the impulse response amplitudes of the output to the input for a given time interval. To show gradual change between the levels of activity, he averaged each over a five interval period. This stacked plot of filters, depicted in Appendix E, shows the impulse response curve for a zero time lag and a filter order corresponding to approximately 4 hours.

Clauer [1986] used a great deal of the information revealed in the paper by Bargatze. His work expanded on the work of Bargatze by using other inputs and outputs to show the advantages of the LPF techniques.

The filter amplitudes show patterns which vary with activity levels. At the lower activity levels, intervals 1 to 6, the filters show two peaks of approximately equal amplitude. The lags for these peaks are roughly at 20 and 60 minutes. They are

somewhat variable, taking values for the 20 minute peak from 15 to 30 minutes and for the 60 minute peak from 55 to 70 minutes [Bargatze, 1985:6390]. The filters gradually decay to zero after approximately 2 hours. The peaks of these impulse responses reflect both the driven and unloading model equally, showing the response of the output is related to two separate mechanisms.

The filters from 6 to 18 also have two peaks, but the second peak is significantly larger than the first. The peaks still remain near the 20 and 60 minute established by the first six filters. This range of filters encompasses the moderate range of activity, and indicates that moderate activity is more closely related to the unloading model, where stored energy is released into the auroral electrojets.

Filters 19 to 30 are much different from the previous two groups of filters. They have a single broad peak and takes longer to decay. The peaks of these filters reach their maximum amplitudes near the 20 minute peak of the first two groups. The peaks are much broader, however, and may cover as much as a 30 minute interval. This indicates the driven model dominates at strong geomagnetic activity levels. The slow decay from the peak amplitude is completed in approximately 2.5 hours. The impulse response curve then stays near the zero line, but remains slightly negative until approximately 3.5 hours of lag where it begins to rise again.

The broadening of the 20 minute peak for strong geomagnetic activity levels is not explained completely. A possible explanation is that although the peak at 20 minutes indicates the driven model has taken precedence, the broadening of the peak would suggest an interaction time. The solar wind-magnetosphere coupling actions do not take

place immediately. The broadening may be the result of the solar wind's push into the magnetosphere, and the magnetosphere's impedance to such action.

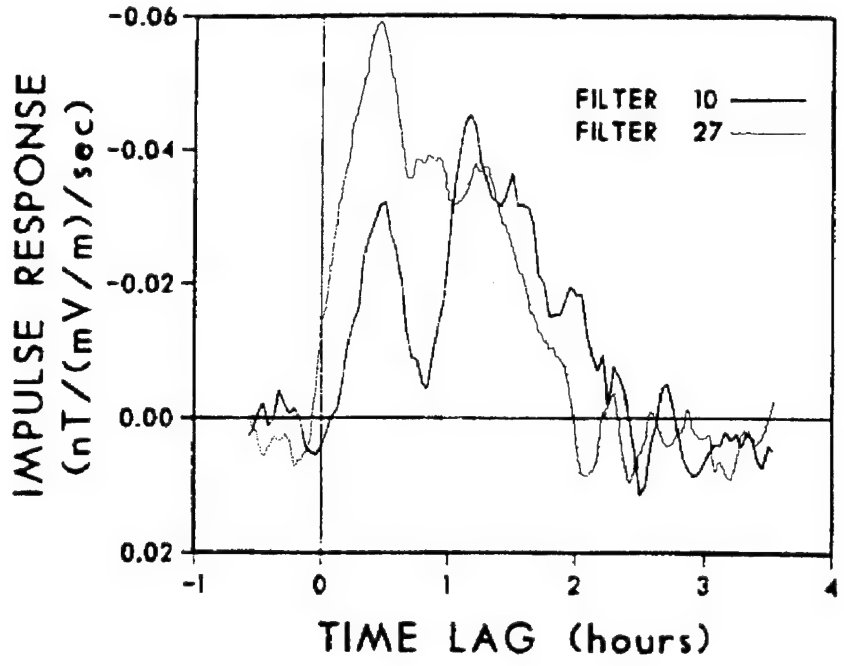

Figure 10. Filters 10 and 27 for the Bargatze data set. (Adopted from Bargatze [1985:6389]).

Filters 10 and 27, reproduced in Figure [10], have been highlighted in Bargatze's paper as representative filters for the second and third group of filters mentioned above. Filter 10 demonstrates the two peak curve with the second peak being higher. Filter 10 describes, in general, the levels of geomagnetic activity where the unloading and driven model are both important to calculation of AL, but the former model is preeminent. Filter 27 illustrates the single peak curve, associated with the dominance of the driven model, with a maxima near the 20 minute lag and decaying gradually thereafter.

Filter and model components

The models used were built by implementing ARMA techniques. The number of previous inputs and outputs and time lags had a great deal of influence on the ability of the model properly estimate the actual output. The papers mentioned earlier do not reference exact values of orders or lags to incorporate into a model in order to maximize its performance. Clauer [1986:43] suggests three courses of action in order to produce the best models possible. They are to set a predetermined length for the model's filter, preset a minimum least squares error for the model to achieve, or continue until the least squares error levels out and shows no sign of any appreciable increase or decrease. The models used in this thesis have set the orders and lags which appear to give the best performance. For single and multiple input models, the best model structure is [10 85 1], where 10 is the number of previous outputs used, 85 the number of previous input data points, and 1 represents the time lag.

Figures 11 and 12 show several intervals where strong activity starts suddenly. The model does not respond quickly to and may miss some onsets of geomagnetic activity. This was also noted by Clauer [1986], so it is not specific to this effort and could be considered as a uncertainity in the physical system or prediction method.

Multiple input models are slightly different than the single input models. The impulse response and model coefficients for multiple input are created with all of the inputs at once. Therefore, their impulse responses and coefficients are very different from those created using single input models. In general, the impulse response curves for the

multiple input models are much smoother than the single input models, and each input affects the impulse response curve differently.

Vassiliadis' [1995] state-input space uses several inputs and outputs in developing the model, and has a different approach to modeling the time series compared to LPF techniques. The state-input space model does not relate to filter estimation or coefficients. The conditions for best fitting a model come from an estimate of distance from a specific point in three dimensional space. This method determines what level of fit is required by the model, and chooses a distance from the reference point which encompasses enough points to give this correlation. The shorter the distance from the reference point to the other points needed to achieve a certain correlation the better the model. The distance can shortened to any minimum length, so long as there is at least one neighbor within that distance. The state-input space model cannot perform its calculations without at least one nearest neighbor. For Vassiliadis' 2.5 hour prediction, use of the three nearest neighbors in state-space produced a model with an average correlation coefficient of 92%.

Residuals and correlations

The comparison of residuals shows the difference between the predicted and actual values for AL. Bargatze et al. [1985] and Vassiliadis et al. [1995] both used residuals as a method of establishing the quality of their results. The results of the predicted values of AL and the residuals from this thesis are seen in Figures 11 and 12. The units of the residuals are the same as the AL index (nT) since they are only the difference between the actual and simulated.

Residuals attained were smaller in overall magnitude than those produced by Bargatze [1986]. Bargatze showed only the results of the model using VB_S as model input to simulate AL. As shown in his paper, the residuals for VB_S over moderate geomagnetic activity levels reached maximum amplitudes near 300 nT. Using the same input and interval of activity, the residuals of this study reach an amplitude slightly less than those of Bargatze, approximately 250 nT. This indicates that this model was better able to fit the data and has a higher correlation since, in areas of low residual amplitudes, the two results are nearly equal.

The results at stronger geomagnetic activity were also superior to those reported by Bargatze, when evaluated in terms of the magnitude of the residuals. Again, over the same time interval and input, this study's residuals did not exceed the amplitude of 400 nT. In contrast, Bargatze's results showed a maximum residual of 600 nT with several peaks over the 400 nT mark. Both sets of residuals show a good deal of departure from the actual AL with the greatest differences occurring at the onset of strong activity. This would indicate that the models did not respond well to sudden increases in the activity level. The models did, however, do reasonably well once the model noticed the increase in activity.

The results of other single input models and multiple input models for moderate and strong geomagnetic activity appear in Appendix C. The models with more than one input show several input graphs, a predicted versus actual AL graph, and a graph of the

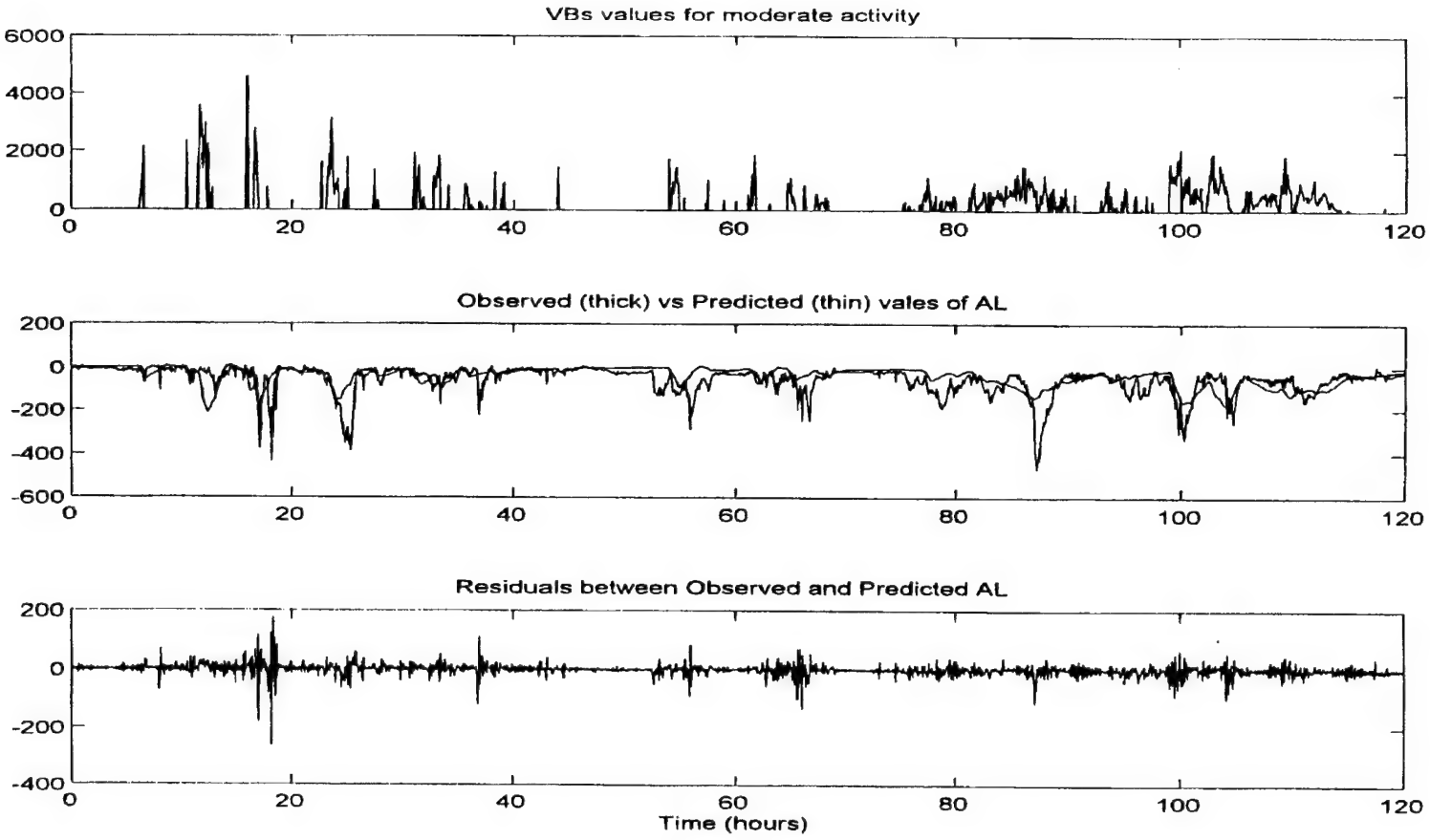

Figure 11. Prediction of AL using VBs (moderate activity).

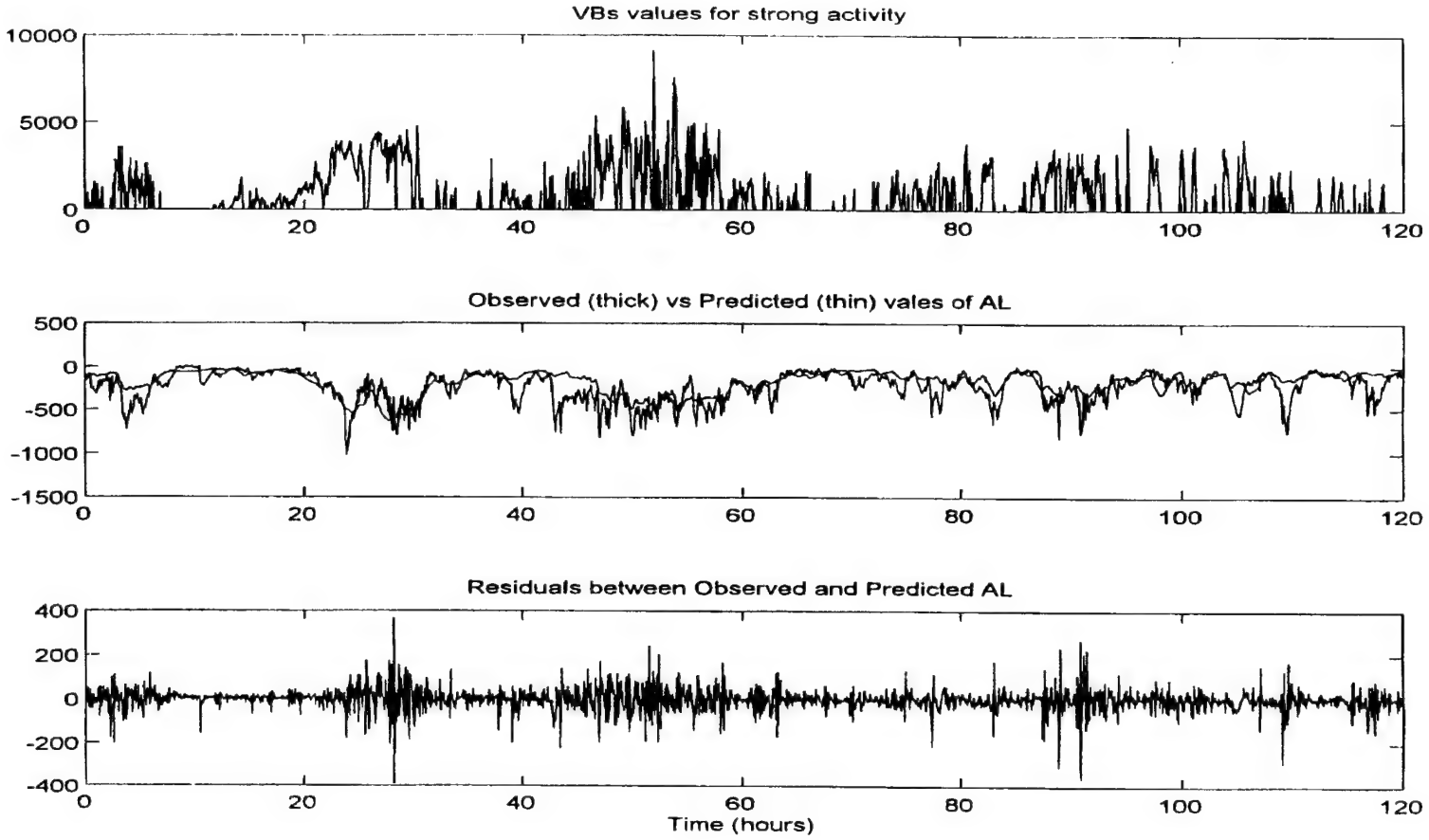

Figure 12. Prediction of AL using VBs (strong activity).

residuals. The combinations of coupling functions and levels of geomagnetic activity can be determined by the titles of each input graph. The figures are numbered and have full title descriptions of the input or inputs, simulated versus actual AL, and the residuals.

The residuals are, in general, smaller for multiple input models. The reason for this is using more than one input allows for modeling multiple reactions of the magnetosphere which have linear contributions to AL. If two or more physical processes are causing the growth or diminishment of AL, models using inputs which involve all of these processes would have a better chance of modeling AL than a model which only involved a single process. This can also be seen in the increase of the correlation for multiple input models. There is an approximate 5% increase in the overall correlation for each model that incorporates an additional input in predicting AL. If a model uses three coupling functions as input, the correlation can be expected to increase by approximately 10%.

Vassiliadis' work shows a remarkable increase in correlation when compared to any of the models which used LPF techniques. His average correlation values were near 94%, while those of Bargatze averaged between 50% and 65% [Vassiliadis, 1995]. This improvement may not be solely due to Vassiliadis' use of state-input space models, but also lie in the fact that he used multiple inputs. If this is the case, linear modeling may be sufficient to produce excellent results, given that the coupling functions have some type of linear relationship to AL or any other geomagnetic index.

The correlation between predicted and observed values of the AL index for various models is presented in Figure 13. The results displayed include Bargatze's single input, this study's single and two multiple input, and Vassiliadis's state-input space correlation

values. In Appendix D, the correlation values reported are those of Bargatze as reported by Vassiliadis, the single input model for VB_S, two multiple input models, and the state-input space model used by Vassiliadis et al [1995]. It is easy to see that the state-input space model "scored" the best of the models tested. The explanation for the improved performance is the nonlinear model was able to interpret relations which the linear models could not, and multiple, instead of single, inputs were used. As seen by both the linear and nonlinear models, an increased number of inputs allows the models to achieve a greater correlation and accuracy compared to single input models.

Vassiliadis et al. [1995] reported that linear prediction filtering averaged 50-60% for cross correlations using single inputs. The single input, LPF, models designed in this thesis achieved correlations in this range. However, the multiple input models show a significant improvement over the single input correlations. The triple input LFP model did quite well with values averaging in the middle to upper 70% range. It is apparent that the next generation of models will need to include both the adaptive and nonlinear features as well as multiple inputs to perform more successfully than those illustrated here.

Forecasting

The method of forecasting AL is very similar to the predictive method used in all of the models described above. The models predict the next value of AL from the coupling function inputs and the previous values of AL. In order to extend this forecast beyond a single time step, different techniques are available.

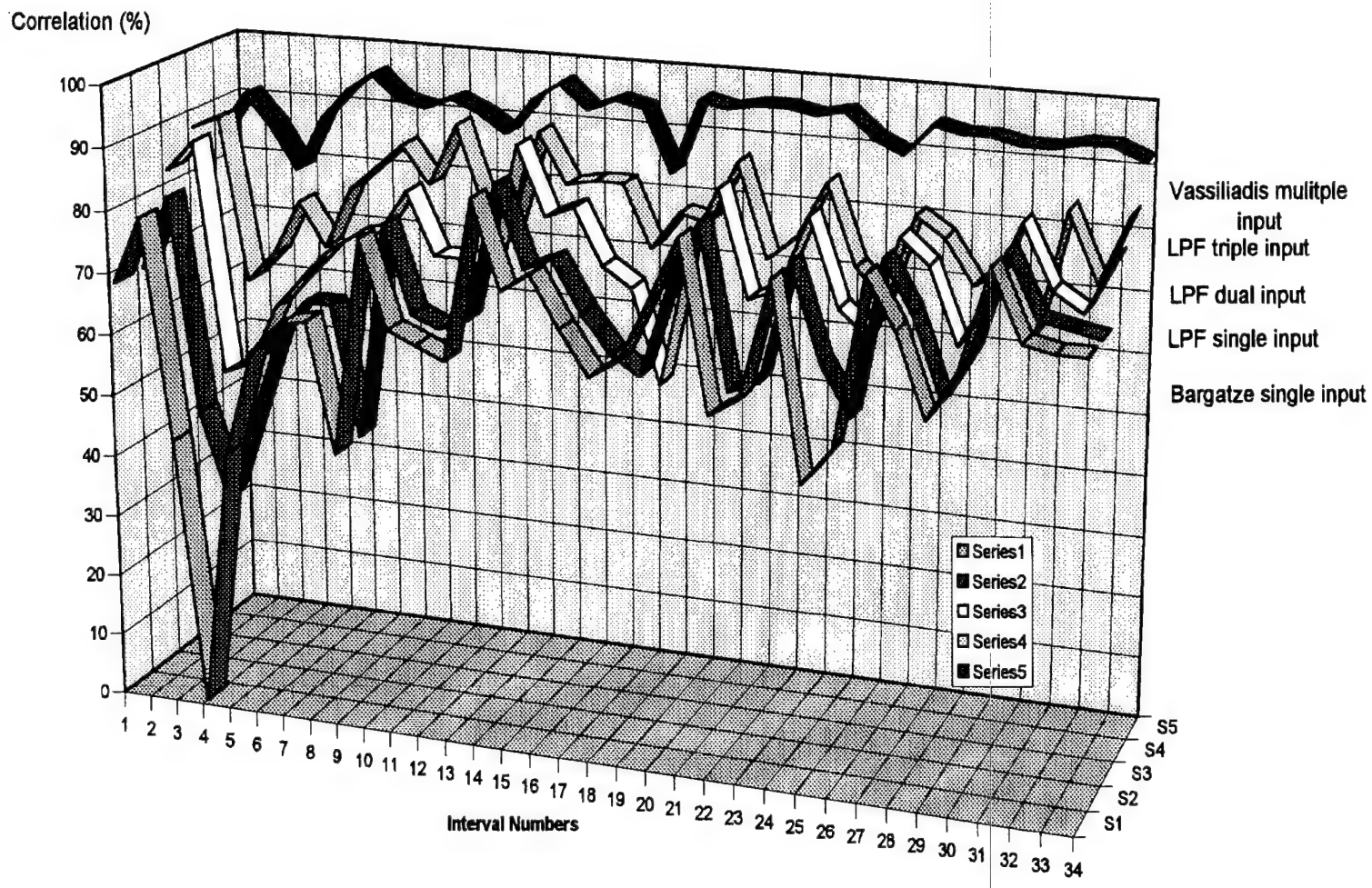

Figure 13. Correlations of various models used.

Two types of forecasting were implemented in this thesis. The first was an extended single step prediction which, in effect, was the same as the prediction of AL produced by the standard LPF models. The distinguishing feature was that the predicted output was now treated as the true, observed value with autoregressive feedback being now driven by a prediction. The input data stream, solar wind data, was assumed to still be available at the 2.5 minute intervals. The second forecast type assumed that both the observed outputs and inputs were not available over the forecast interval. Operationally, when those conditions are encountered, persistance of the output is the standard forecast. However, improving on this, within the LPF approaches, requires that inputs be supplied. The remedy adapted was input persistance.

The basis of the input persistance method is the distributed nature of the impulse response. Previously, we established that significant contributions to the impulse response extended over a time interval in excess of 90 minutes, with "peak" contributions at lagged times of 25 and 70 minutes. Forecasts using only lagged input values in the 30 to 70 minute sector of the true input data, for example, would capture a significant portion of the impulse response. Filling the remaining interval, if the fill is chosen appropriately, will improve the prediction and enable a time interval forecast, t_f (30 minutes in this example). The implementation of input persistance thus consists of repeating or duplicating the input data (persistance) over a time interval for forecast, t_f, and using this current data, from current time t through $t-t_f$, as the future data for t to $t + t_f$.

These forecast methods produced results which were better correlated than persistance but less accurate than the model's prediction at short time increments. The results showed residuals ranging from 175 to 400 nT for low to moderate activity for both models and, for strong activity, ranging from 500 to 800 nT for the single step method and 500 to 950 nT for the input persistance method. The cross correlation values between the forecast and actual values of AL for both methods ranged from 0.69 at low levels to 0.35 for strong geomagnetic activity. On average, the single step method performed between 0.03 and 0.06 better than the input persistance method.

Vassiliadis et al. [1995] predicted AL in single steps out to the desired forecast time. Using each new predicted value of AL as a previous value, he then predicted the next value of AL using the actual inputs and their nearest neighbors in state-input space. In this approach, the two limitations on single step predictions are 1) the amount of noise in the data and the determinism of the coupling and 2) the amount of available data in the region of interest in the state-input space [Vassiliadis et al., 1995:3498]. As seen in Figure 13, the correlations of the 2.5 minute prediction were the highest, by far, of all of the models. The values for the 4.17 hour prediction model were lower but in the same range as the dual and triple input models for linear prediction filtering.

V. Conclusions and Recommendations

This chapter will be concise as it contains only two sections. The first will assess the models developed, discuss limitations and achievements, and compare them to previous work in the field. The second section will introduce directions to follow in order to further this research and suggest even better methods for predicting the desired indices.

Conclusions

There are several conclusions which can be drawn from the results of this research. Some of them include the use of LPF in prediction and forecasting, the accuracy of LPF in comparison to other linear and nonlinear models, and the limitations of the LPF in forecasting.

The techniques of linear prediction filtering represent a useful tool and can be used to develop good models for predicting geomagnetic activity. The impulse response curves for the different coupling functions provide physical insight regarding characteristic system times and enable assessment of physical mechanisms and models. Multiple input models allow the LPF techniques to achieve improved correlation scores and lower residuals when compared to single input models. The effectiveness of these LPF approaches, however, has already been surpassed by the use of state-input space models. Other techniques capable of addressing nonlinear systems becoming available, such as neural networks, should be used to examine the physical processes of solar wind-magnetosphere coupling.

LPF methods developed in this effort showed good comparisons to the results of the previous linear methods as well as the state-input space models. The past linear models were able to achieve correlations of approximately 60 with the actual values of AL while the linear models of this thesis reach an average 78 using three inputs. The state-input space model, also using three inputs, achieved much better results, nearly 94% of the actual AL values. The LPF methods results are excellent for linear models, but it can be seen that nonlinear methods should be employed to secure the best results.

An obvious limitation of LPF techniques is they model only the linear processes which take place. It is clear that some of the processes in the solar wind-magnetosphere coupling are nonlinear. Therefore, nonlinear models are the best equipped to model and forecast them.

Recommendations

There are several directions to take to continue this research. They involve using different types of models, applying these methods to different indices, and using other coupling functions discussed by Gonzalez [1990] to determine their importance with respect to all of the different indices. Such investigations will provide substantial progress for the field of predicting the geomagnetic indices and a better understanding of the processes taking place during the coupling of the solar wind and magnetosphere.

Application of adaptive filtering techniques to nonlinear methods is a good place to start additional research. Nonlinear methods should show a greater correlation between the solar wind input and the resulting indices. In the last several years, neural networks

have been experimented with and refined to a degree which suggests their use would be beneficial in the arena of forecasting. They are able to model linear as well as nonlinear effects in a continuous time domain. This makes them very applicable to the prediction and forecasting of geomagnetic indices. Their application to this field should be studied, applied, and exploited.

The different indices represent varied effects taking place within the overall coupling between the solar wind-magnetosphere system. By modeling each of the indices with adaptive filtering techniques, understanding can be gained for both the physical actions taking place and the relative linear-nonlinear relationship between the indices and the solar wind input. By using different coupling functions in the prediction of different indices, new indications of the processes taking place may be revealed.

APPENDIX A: Data Formats

Data Format for Bargatze Data Set

The Bargatze data set is a matrix which is 42216 x 14 in dimension. The number of rows (42216) is the number of 2.5-minute time steps in the interval. The numbers of columns (14) are the types of data in the set itself. Below, listed by column number, are the data which are included in the Bargatze set:

1. TIME in YYMMDDSSSSS format where YY is the two digit year (i.e. 67 is 1967), MM is the month, DD is the day of month, and SSSSS is the seconds of day which ranges between 00000 and 86250 for this 2.5 minute data set.

2. AE Index in nT

3. AL Index in nT

4. X coordinate of IMP 8 in GSM coordinates and in km

5. Y coordinate of IMP 8 in GSM coordinates and in km

6. Z coordinate of IMP 8 in GSM coordinates and in km

7. Bx in GSM coordinates and in nT

8. By in GSM coordinates and in nT

9. Bz in GSM coordinates and in nT

10. B sigma squared in (nT)**2, a measure of the magnetic field variance

11. Np, the proton number density in #/cm**3

12. V, the solar wind bulk speed in km/s

13. Na, the alpha particle number density in #/cm**3

14. Tp, the proton temperature in degrees K

Data Format for Solar Wind Experiment (SWE) data

The following format statement can be used to read the SWE data into a Fortran program. The data itself is an XX x 24 matrix. The length is dependent on how long a window remains open while receiving the data. The data in each column is described in the list below.

Fortran Code

```
READ(1,100) IYRDAY,UTIME,MILLSEC,DATA(I),I=1,20)
100 FORMAT(I6,1X,A12,I9,20F12.3)
```

Column listing

1	GSM VX	KM/S	WIND KP DATA: SWE GSM VX
2	GSM VY	KM/S	WIND KP DATA: SWE GSM VY
3	GSM VZ	KM/S	WIND KP DATA: SWE GSM VZ
4	GSM VT	KM/S	WIND KP DATA: SWE GSM VT
5	GSM VTHETA	DEG	WIND KP DATA: SWE GSM VTHETA
6	GSM VPHI	DEG	WIND KP DATA: SWE GSM VPHI
7	GSE VX	KM/S	WIND KP DATA: SWE GSE VX
8	GSE VY	KM/S	WIND KP DATA: SWE GSE VY
9	GSE VZ	KM/S	WIND KP DATA: SWE GSE VZ
10	GSE VTHETA	DEG	WIND KP DATA: SWE GSE VTHETA
11	GSE VPHI	DEG	WIND KP DATA: SWE GSE VPHI
12	DISTANCE	RE	WIND DIST: S/C DISTANCE
13	GSM RX	RE	WIND GSM RX: S/C POSITION
14	GSM RY	RE	WIND GSM RY: S/C POSITION
15	GSM RZ	RE	WIND GSM RZ: S/C POSITION
16	GSE RX	RE	WIND GSE RX: S/C POSITION
17	GSE RY	RE	WIND GSE RY: S/C POSITION
18	GSE RZ	RE	WIND GSE RZ: S/C POSITION
19	ATEMP	DEG K	WIND KP DATA: SWE PROTON TEMP
20	ADENS	P/CM3	WIND KP DATA: SWE PROTON DENS

Data Format for Magnetic Field Instrument (MFI) data

The following format statement can be used to read the MFI data into a Fortran program. The data itself is an XX x 20 matrix. The length is dependent on how long a window remains open while receiving the data. The data in each column is described in the list below.

Fortran Code

```
READ(1,100) IYRDAY,UTIME,MILLSEC,DATA(I),I=1,18)
100 FORMAT(I6,1X,A12,I9,18F12.3)
```

Column listing

1	GSM BX	NT	WIND KP DATA: GSM BX
2	GSM BY	NT	WIND KP DATA: GSM BY
3	GSM BZ	NT	WIND KP DATA: GSM BZ
4	GSM BT	NT	WIND KP DATA: GSM BT
5	GSM BTHETA	DEG	WIND KP DATA: GSM BTHETA
6	GSM BPHI	DEG	WIND KP DATA: GSM BPHI
7	GSE BX	NT	WIND KP DATA: GSE BX
8	GSE BY	NT	WIND KP DATA: GSE BY
9	GSE BZ	NT	WIND KP DATA: GSE BZ
10	GSE BTHETA	DEG	WIND KP DATA: GSE BTHETA
11	GSE BPHI	DEG	WIND KP DATA: GSE BPHI
12	DISTANCE	RE	WIND DIST: S/C DISTANCE
13	GSM RX	RE	WIND GSM RX: S/C POSITION
14	GSM RY	RE	WIND GSM RY: S/C POSITION
15	GSM RZ	RE	WIND GSM RZ: S/C POSITION
16	GSE RX	RE	WIND GSE RX: S/C POSITION
17	GSE RY	RE	WIND GSE RY: S/C POSITION
18	GSE RZ	RE	WIND GSE RZ: S/C POSITION

APPENDIX B: Bargatze Data Set Information

Intervals of the Bargatze data set

(From Dr. Klimas, Personal Correspondence)

Interval number	Beginning-End (in Points)	Beginning-End (in Hours)	Number of Points (in Interval)
1	1-660	0-27.5	660
2	660-1596	27.5-66.5	936
3	1596-2592	66.5-108.0	996
4	2592-3264	108.0-136.0	672
5	3264-4068	136.0-169.5	804
6	4068-4956	169.5-206.5	888
7	4956-5940	206.5-247.5	984
8	5940-7212	247.5-300.5	1272
9	7212-7764	300.5-323.5	552
10	7764-9420	323.5-392.5	1656
11	9420-10452	392.5-435.5	1032
12	10452-11064	435.5-461.0	612
13	11064-12324	461.0-513.5	1260
14	12324-13008	513.5-542.0	684
15	13008-14532	542.0-605.5	1524
16	14532-15720	605.5-655.0	1188
17	15720-17160	655.0-715.0	1440
18	17160-18564	715.0-773.5	1404
19	18564-19596	773.5-816.5	1032
20	19596-20532	816.5-855.5	936
21	20532-21708	855.5-904.5	1176
22	21708-22836	904.5-951.5	1128
23	22836-24012	951.5-1000.5	1176
24	24012-24912	1000.5-1038.0	900
25	24912-26124	1038.0-1088.5	1212
26	26124-27876	1088.5-1161.5	1752
27	27876-29796	1161.5-1241.5	1920
28	29796-31812	1241.5-1325.5	2016
29	31812-34476	1325.5-1436.5	2664
30	34476-37104	1436.5-1546.0	2628
31	37104-38148	1546.0-1589.5	1044
32	38148-39660	1589.5-1652.5	1512
33	39660-41460	1652.5-1727.5	1800
34	41460-42216	1727.5-1759.0	756

Bargatze Data Set Components

[Means of the parameters used in computing the various models]

(All calculations were made using double precision accuracy.)

Interval	AL Index	Bs	VBs	V^2Bs	Epsilon
1	-15.227273	0.20492577	67.0471714	21936.3493	573.915282
2	-25.611526	0.51431242	183.263214	65301.565	1645.57648
3	-32.019057	0.19343149	64.947771	21807.2714	1371.04054
4	-33.46211	0.15687739	74.9729211	35830.1405	1455.70048
5	-39.086957	0.23949521	97.4044936	39615.1359	1725.42281
6	-30.56243	0.41618896	174.740152	73366.0032	2078.94568
7	-37.17868	0.70004449	254.090154	92225.2897	2126.45236
8	-47.568735	0.93924617	303.079525	97798.8533	2955.85545
9	-35.799277	0.2955825	117.414416	46640.6008	1972.59965
10	-41.629451	0.43832874	148.41389	50251.5135	1536.57794
11	-45.03485	0.39354822	178.741892	81181.0653	3791.00373
12	-50.587276	0.168572	87.3595636	45272.6046	3042.06145
13	-69.458366	0.63473358	280.656093	124095.913	4335.40463
14	-66.252555	0.98601463	353.110321	126455.425	5066.58246
15	-78.161967	0.99907416	407.318642	166062.224	4294.00479
16	-89.783011	0.88939006	389.951065	170973.166	4587.83306
17	-106.84178	0.67115191	319.716843	152303.612	5962.70139
18	-101.59359	0.61629239	319.185418	165310.058	4757.23215
19	-96.736689	1.56116573	657.623398	277016.415	8385.39901
20	-83.116329	1.11901064	490.158559	214703.421	4539.01254
21	-128.42991	2.46372657	893.24006	323849.982	14215.3971
22	-102.69619	1.20490582	579.212238	278434.059	8913.44441
23	-133.12234	1.72903147	709.895004	291464.282	9212.53151
24	-150.37292	1.42075298	640.076672	288366.909	7087.67384
25	-152.65293	1.06904252	620.804525	360507.887	9957.54564
26	-186.28694	0.67888426	484.125901	345239.835	6088.12426
27	-204.09058	0.86835436	556.750409	356963.739	8528.96208
28	-218.17353	0.9823384	660.402298	443972.457	10818.8573
29	-227.37186	1.02337076	633.85389	392595.499	13397.5192
30	-231.77025	1.73080193	935.914742	506087.029	15770.8044
31	-247.61818	2.0296073	1195.09673	703710.617	15817.4818
32	-289.64706	1.394705	831.035612	495172.948	8053.17499
33	-287.82954	1.44331395	883.076023	540300.509	7390.91338
34	-413.08851	3.50311121	1825.23298	951004.755	34588.5883

Appendix C: Simulation of AL using various models

The following figures are numbered and included as references. Each has one or more titles and descriptions to allow the reader a better understanding of what is contained and how they would be applicable.

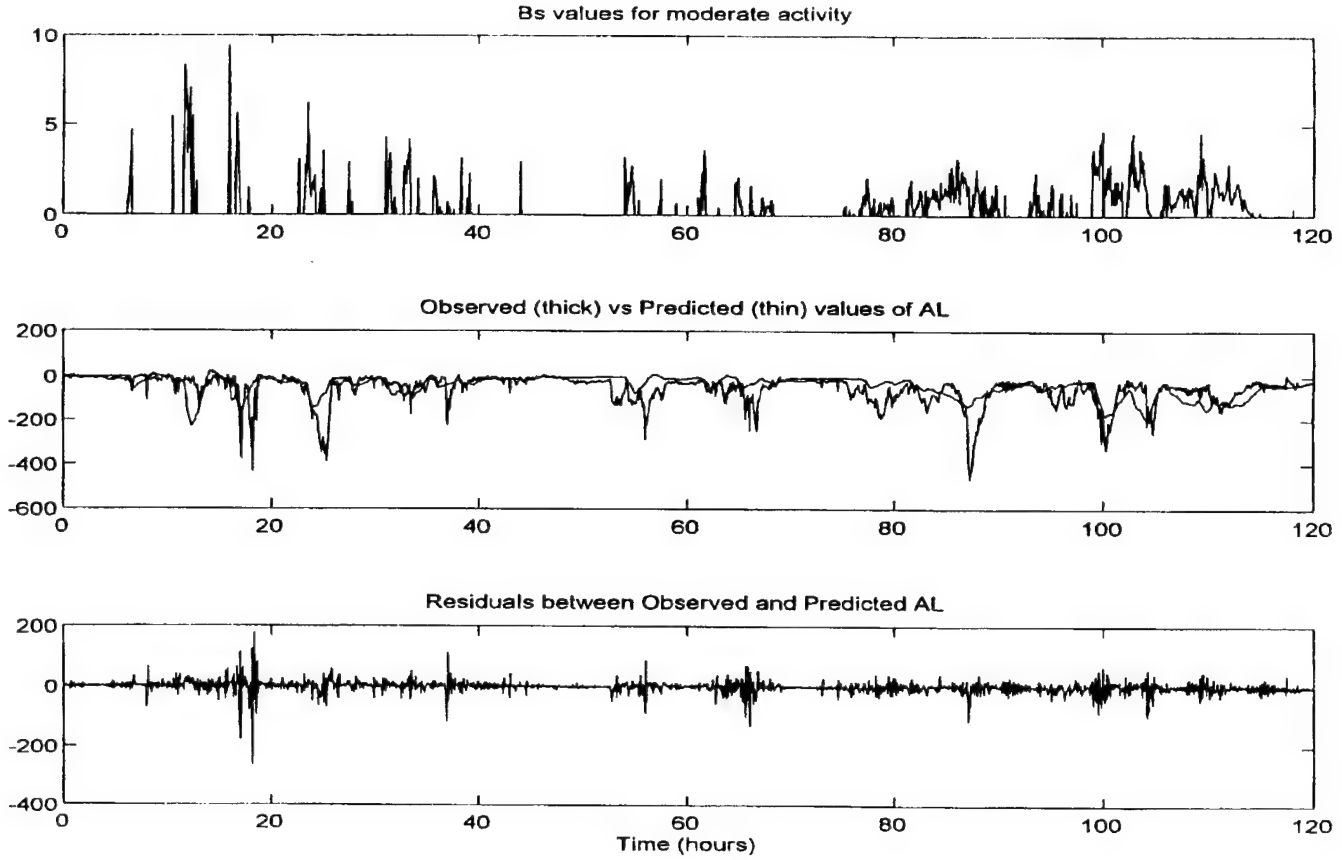

Figure C1. Single input model for Bs. (moderate activity).

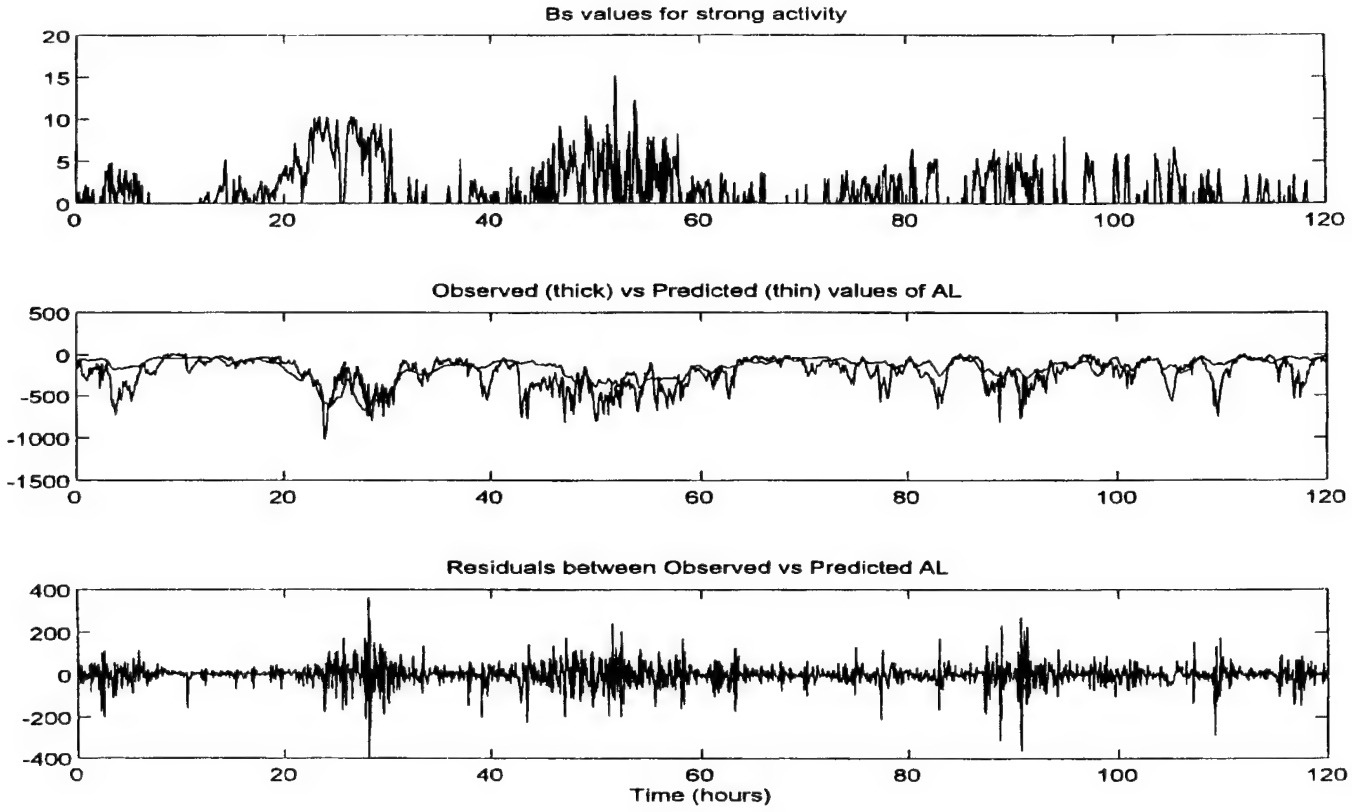

Figure C2. Single input model for Bs. (strong activity).

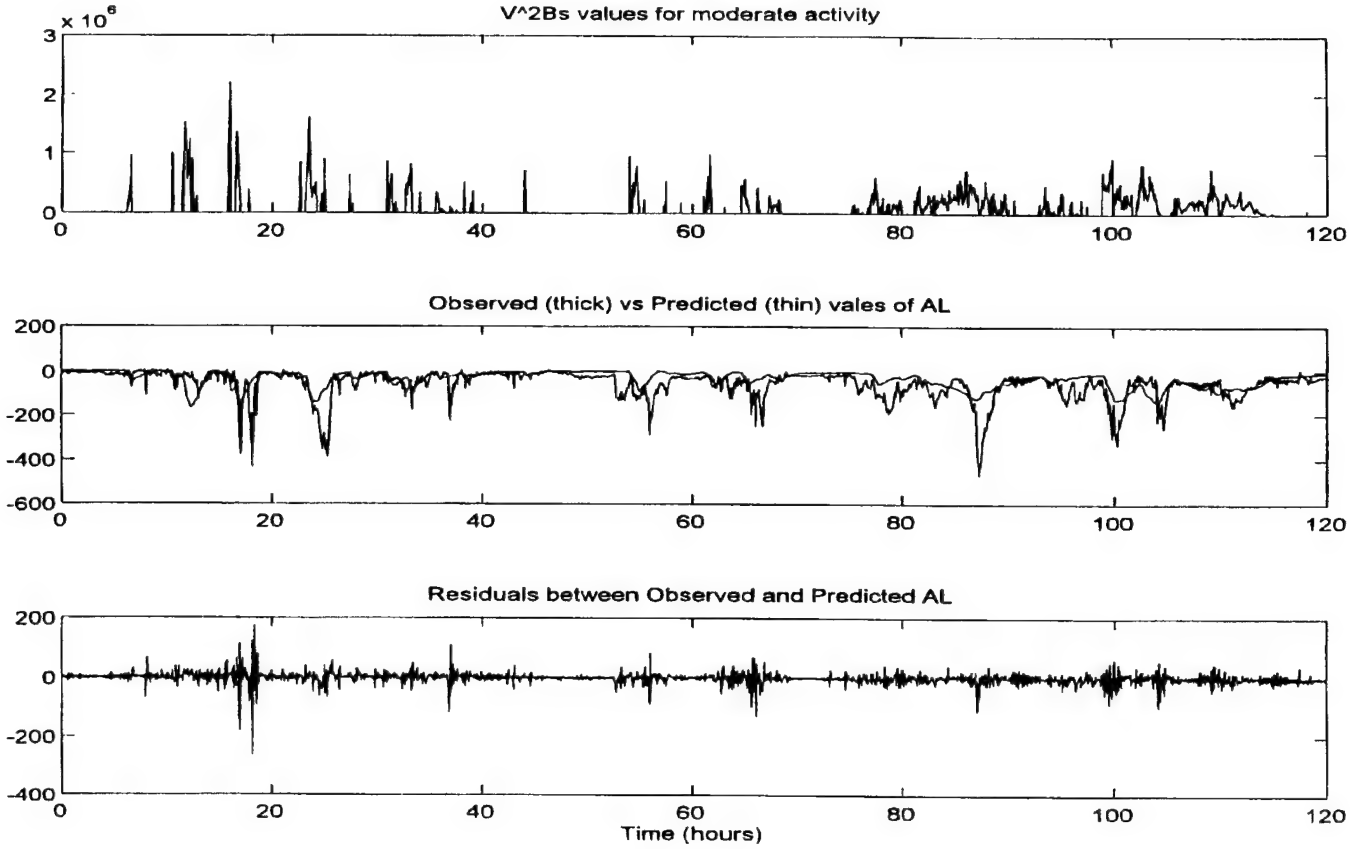

Figure C3. Single input model for V^2Bs. (moderate activity).

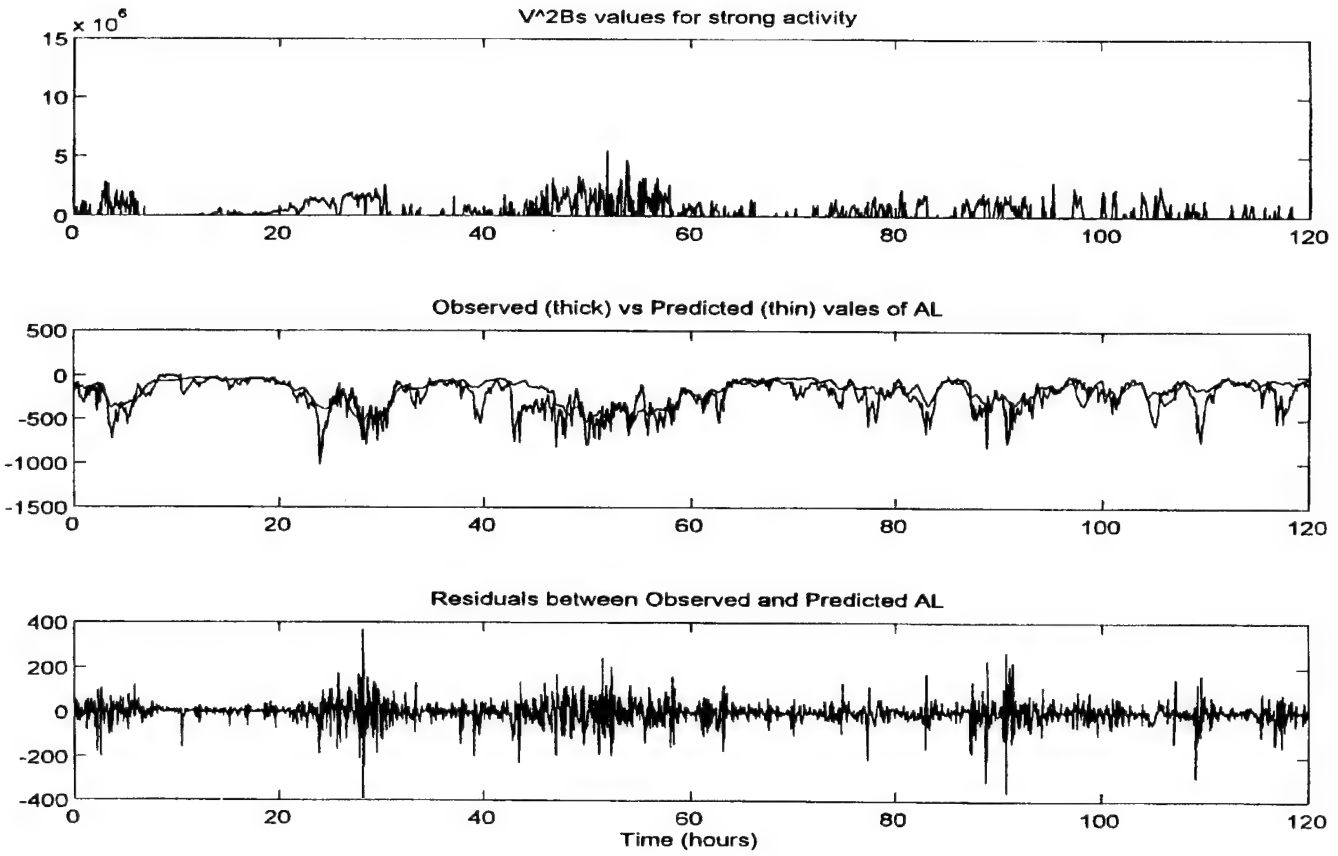

Figure C4. Single input model for V^2Bs. (strong activity).

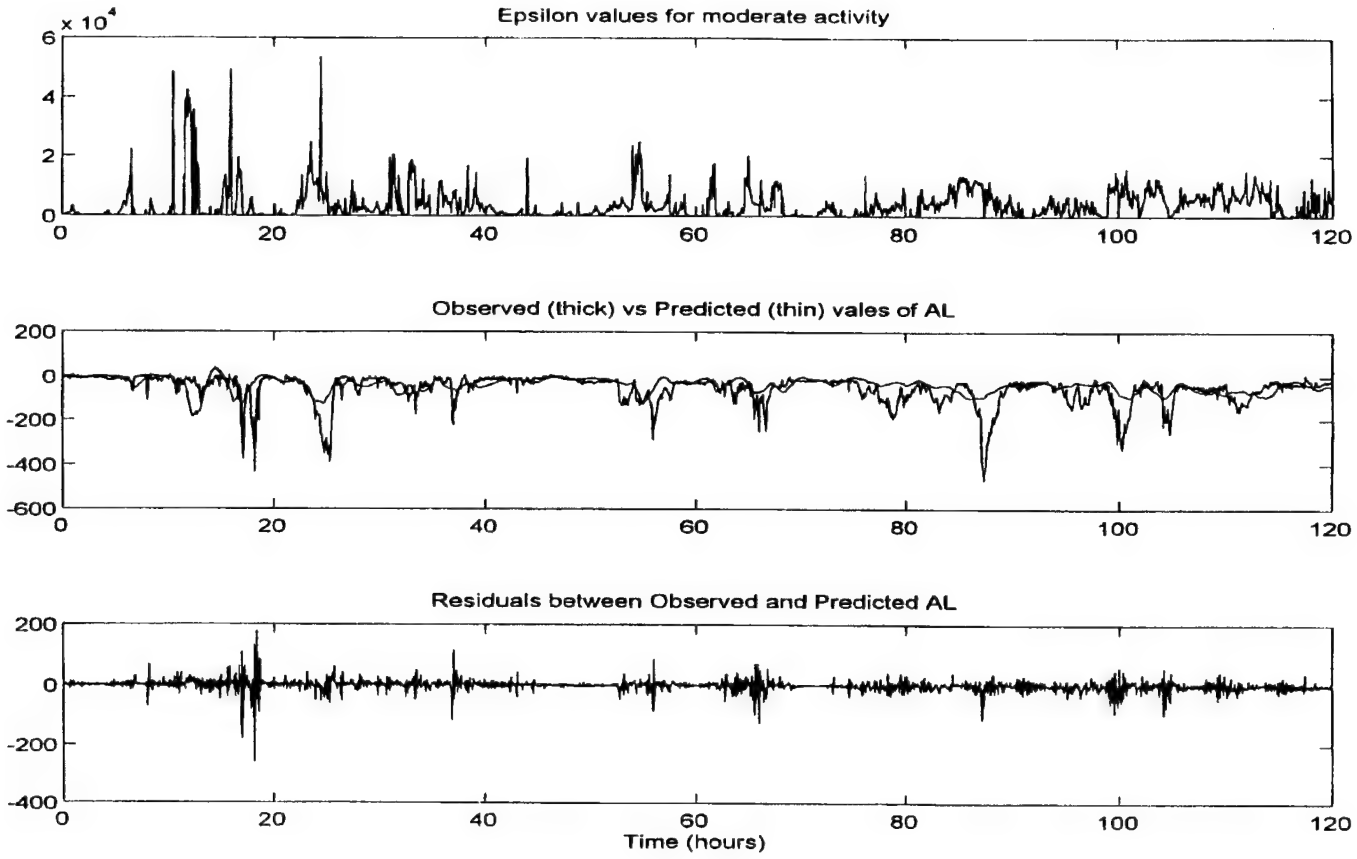

Figure C5. Single input model for Epsilon. (moderate activity).

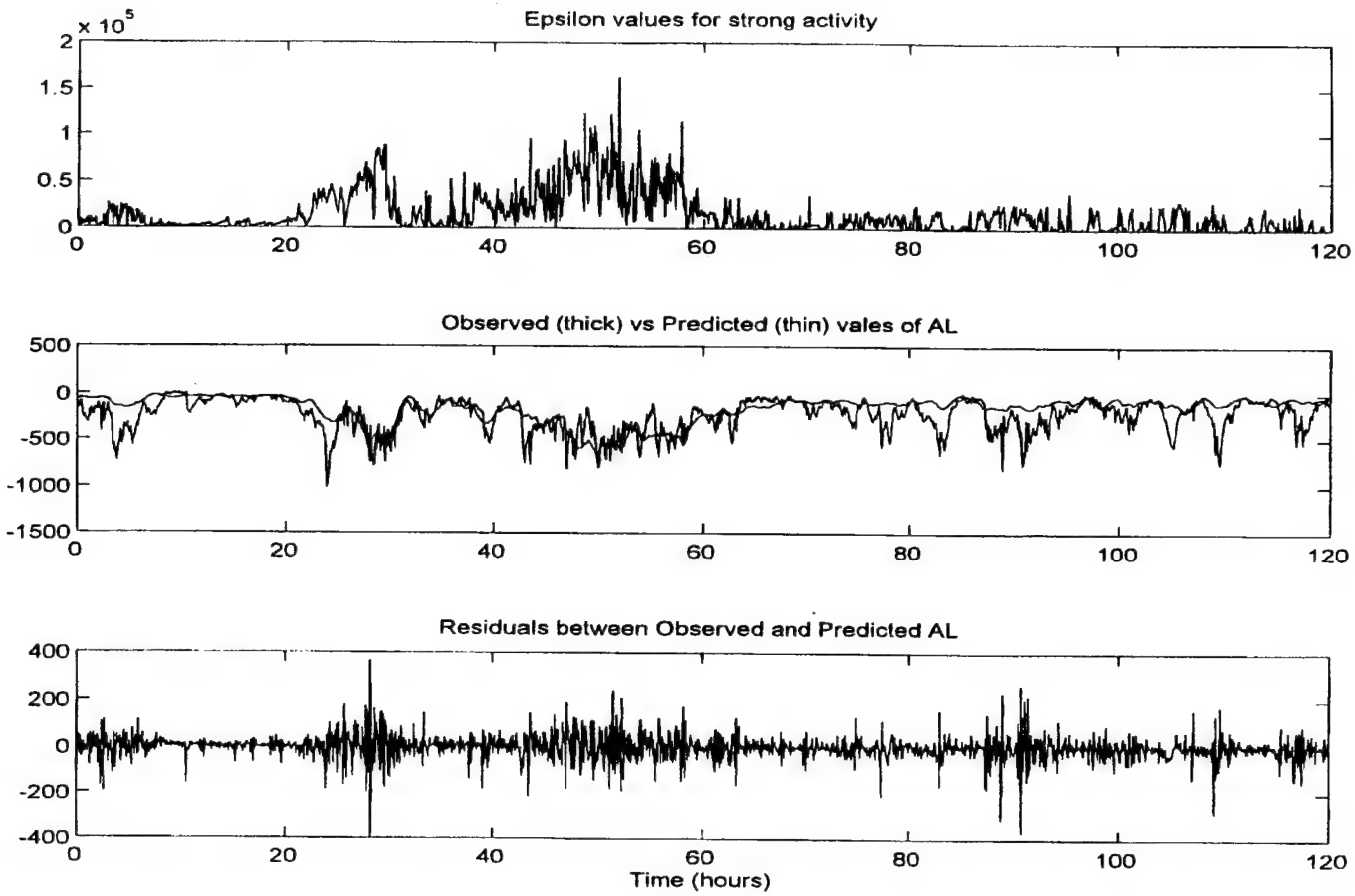

Figure C 6. Single input model for Epsilon. (strong activity).

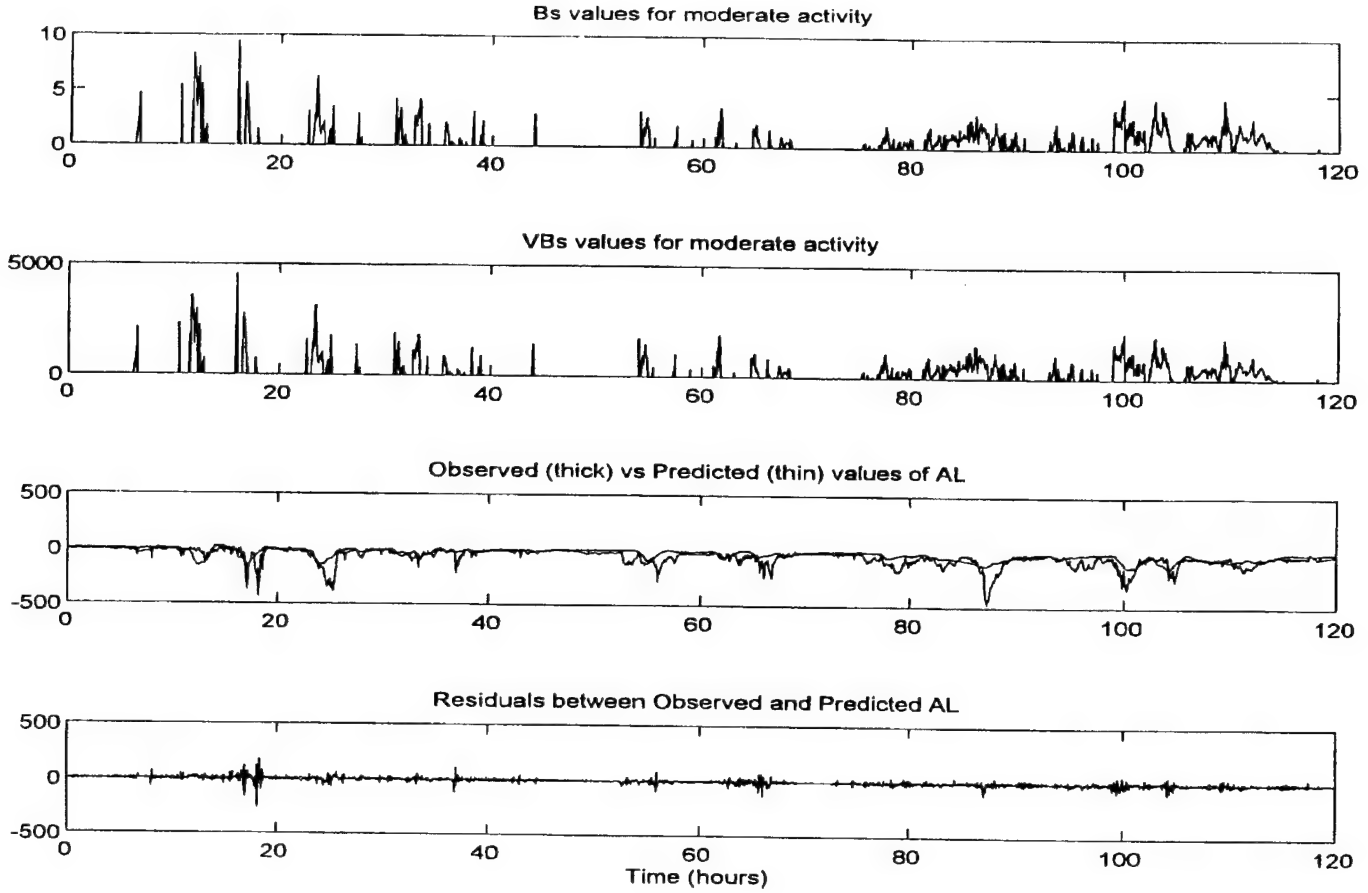

Figure C7. Multiple input model for Bs and VBs. (moderate activity).

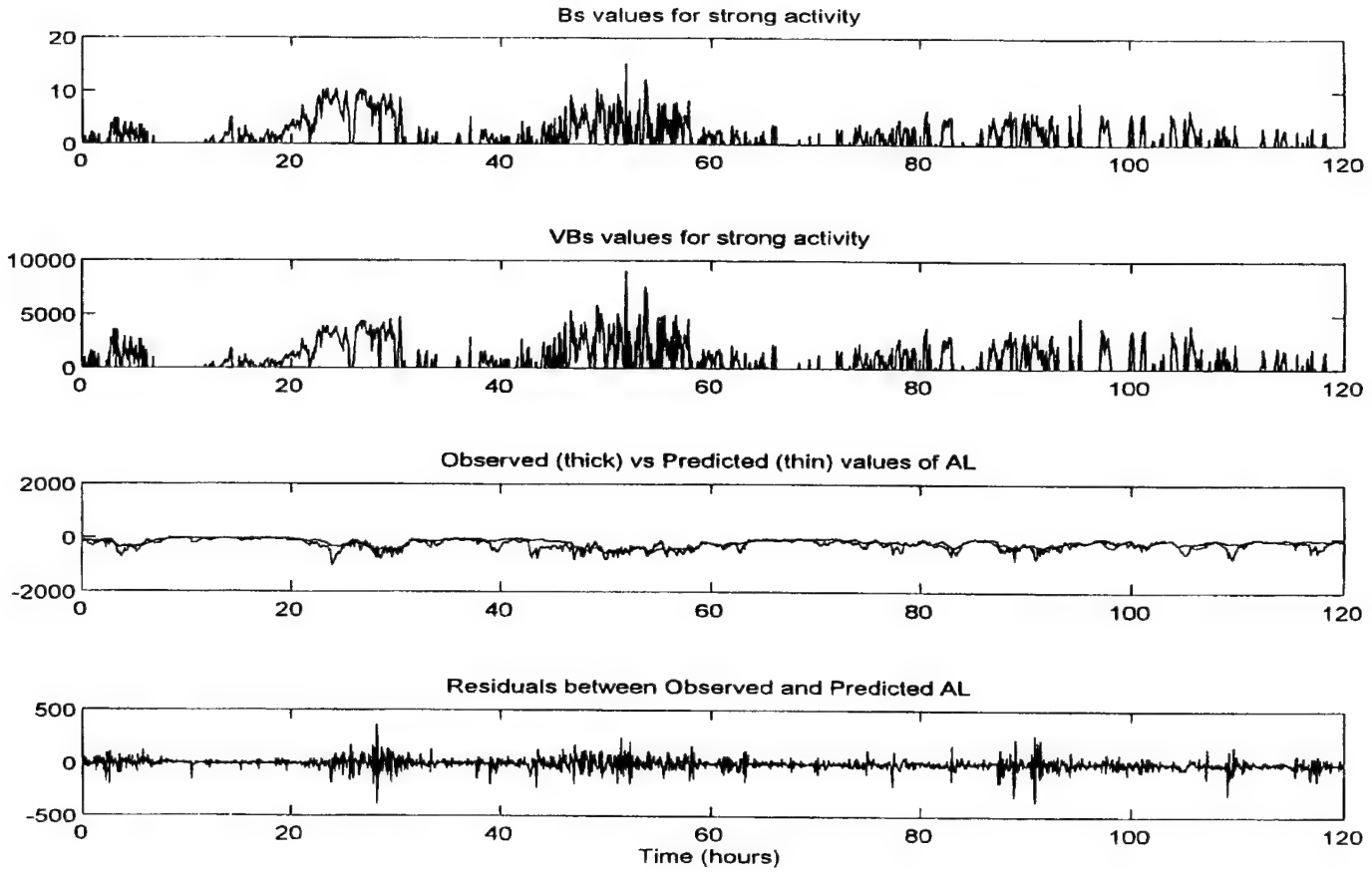

Figure C8. Multiple input model for Bs and VBs. (strong activity).

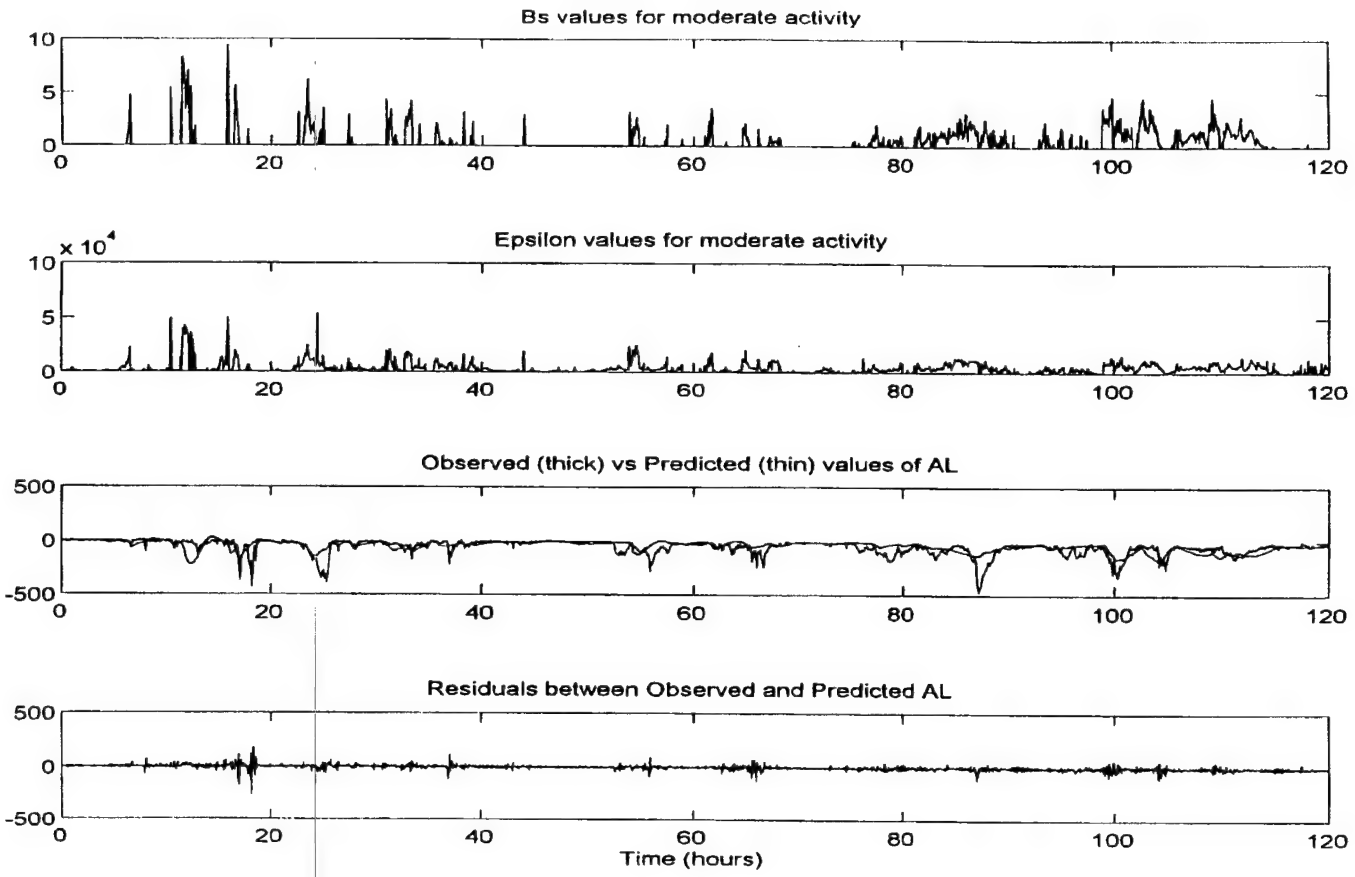

Figure C9. Multiple input model for Bs and Epsilon (moderate activity).

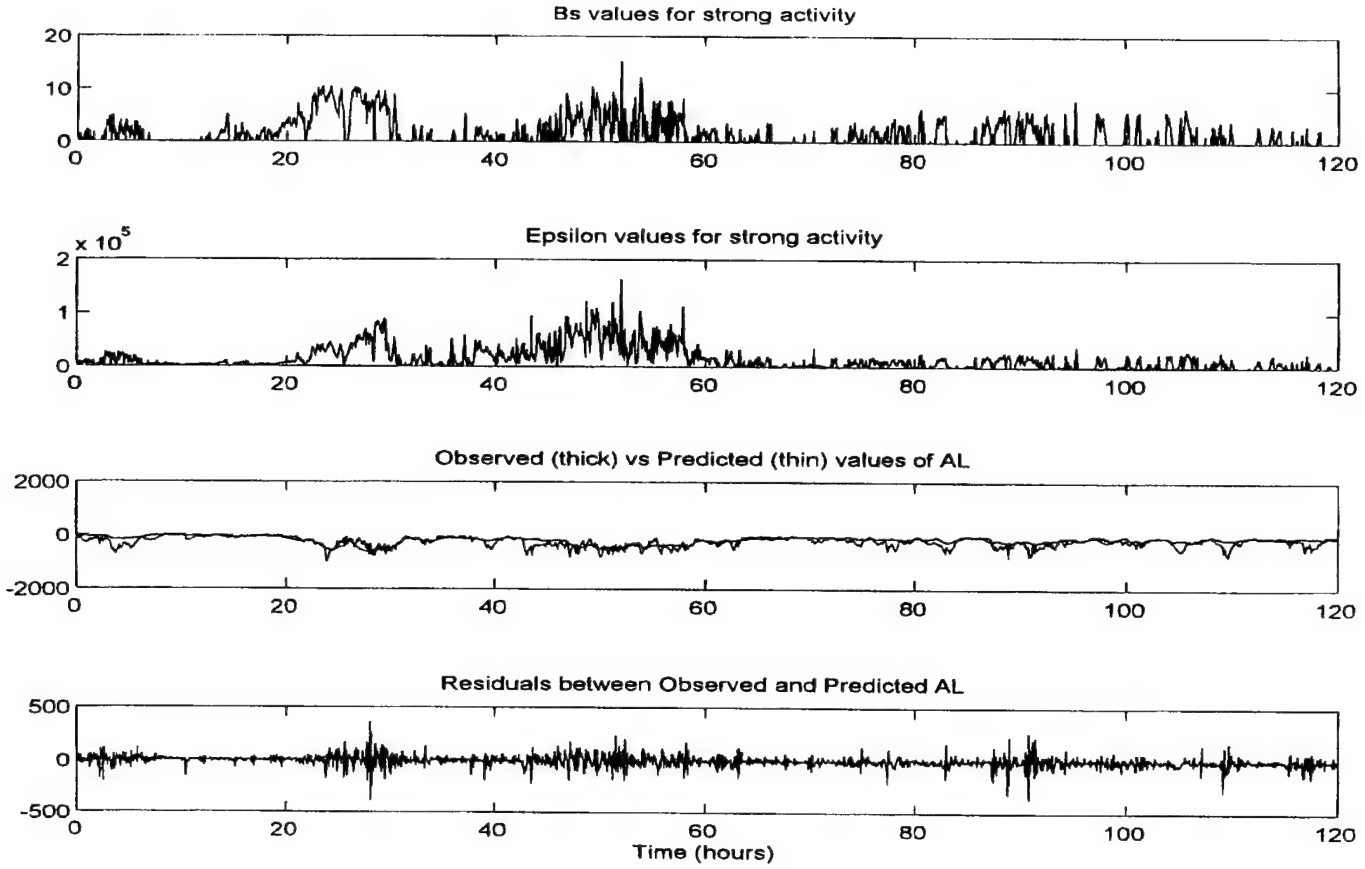

Figure C10. Multiple input model for Bs and Epsilon (strong activity).

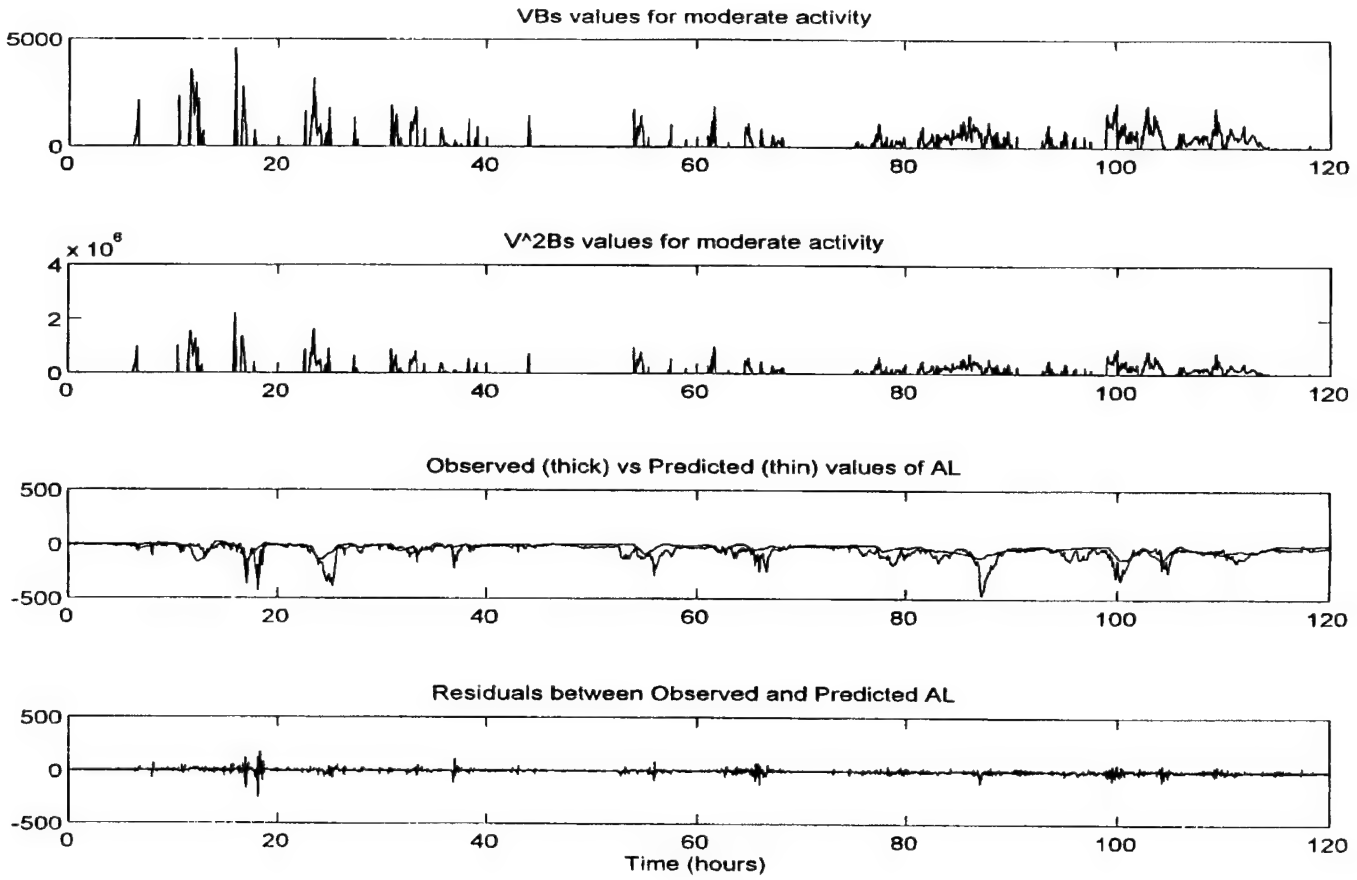

Figure C11. Multiple input model for VBs and V^2Bs (moderate activity).

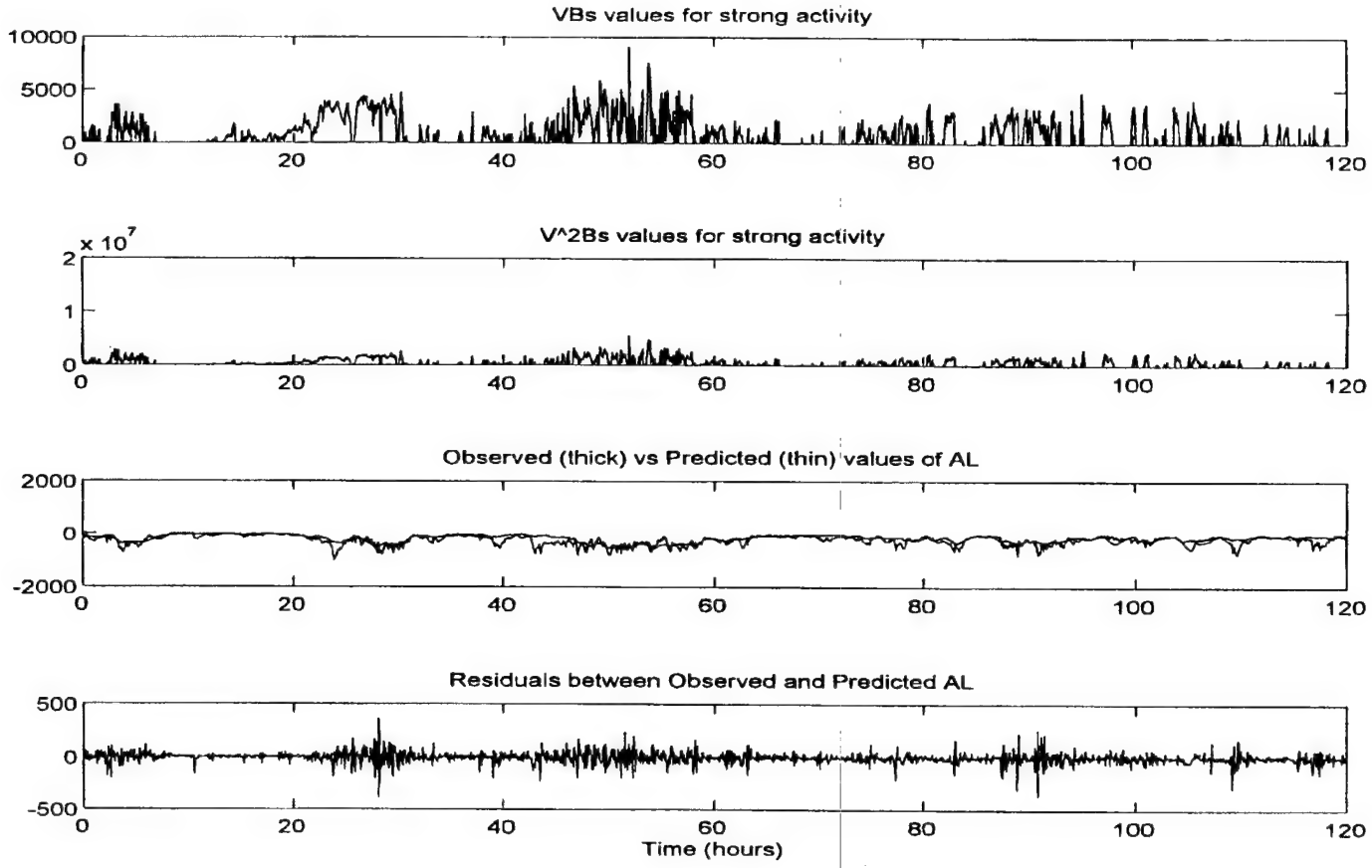

Figure C12. Multiple input model for VBs and V^2Bs (strong activity).

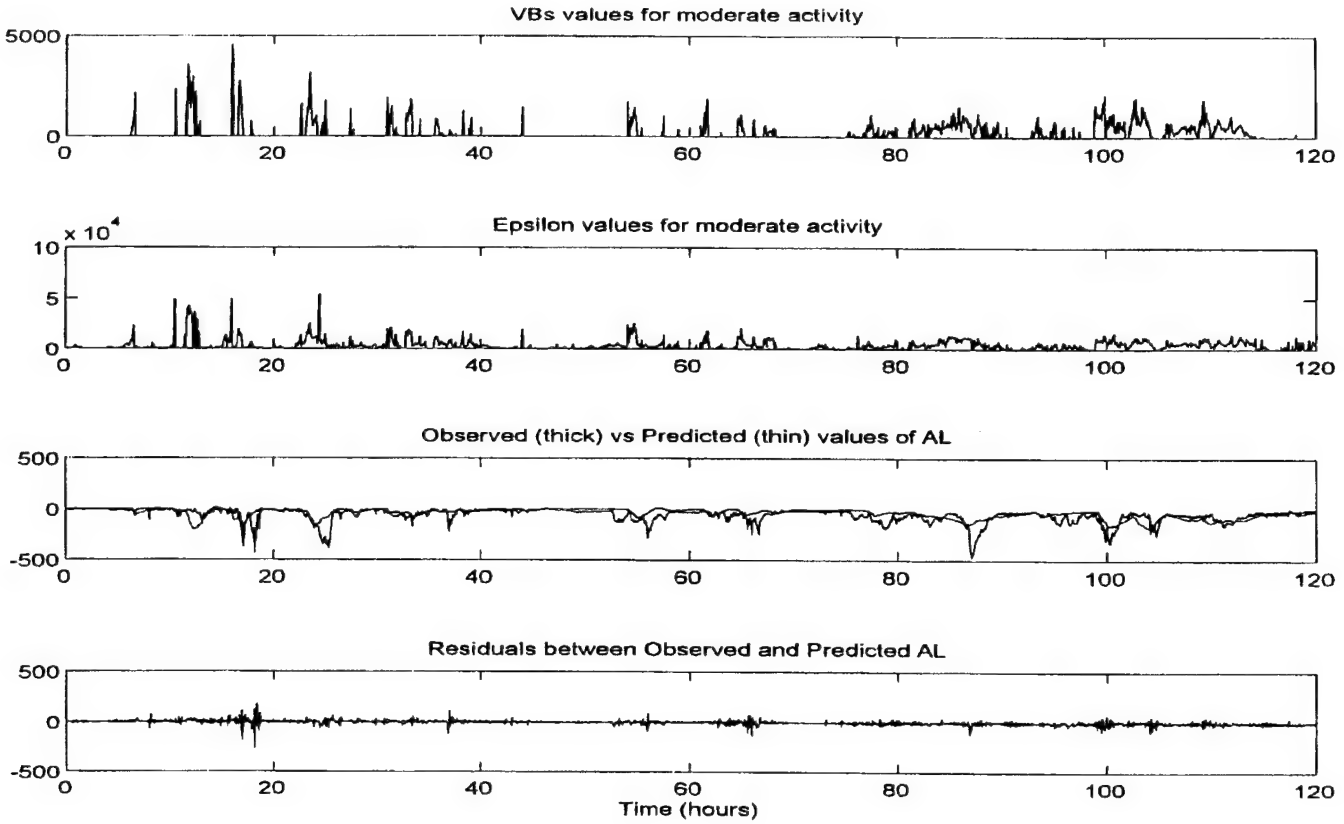

Figure C13. Multiple input model for VBs and Epsilon (moderate activity).

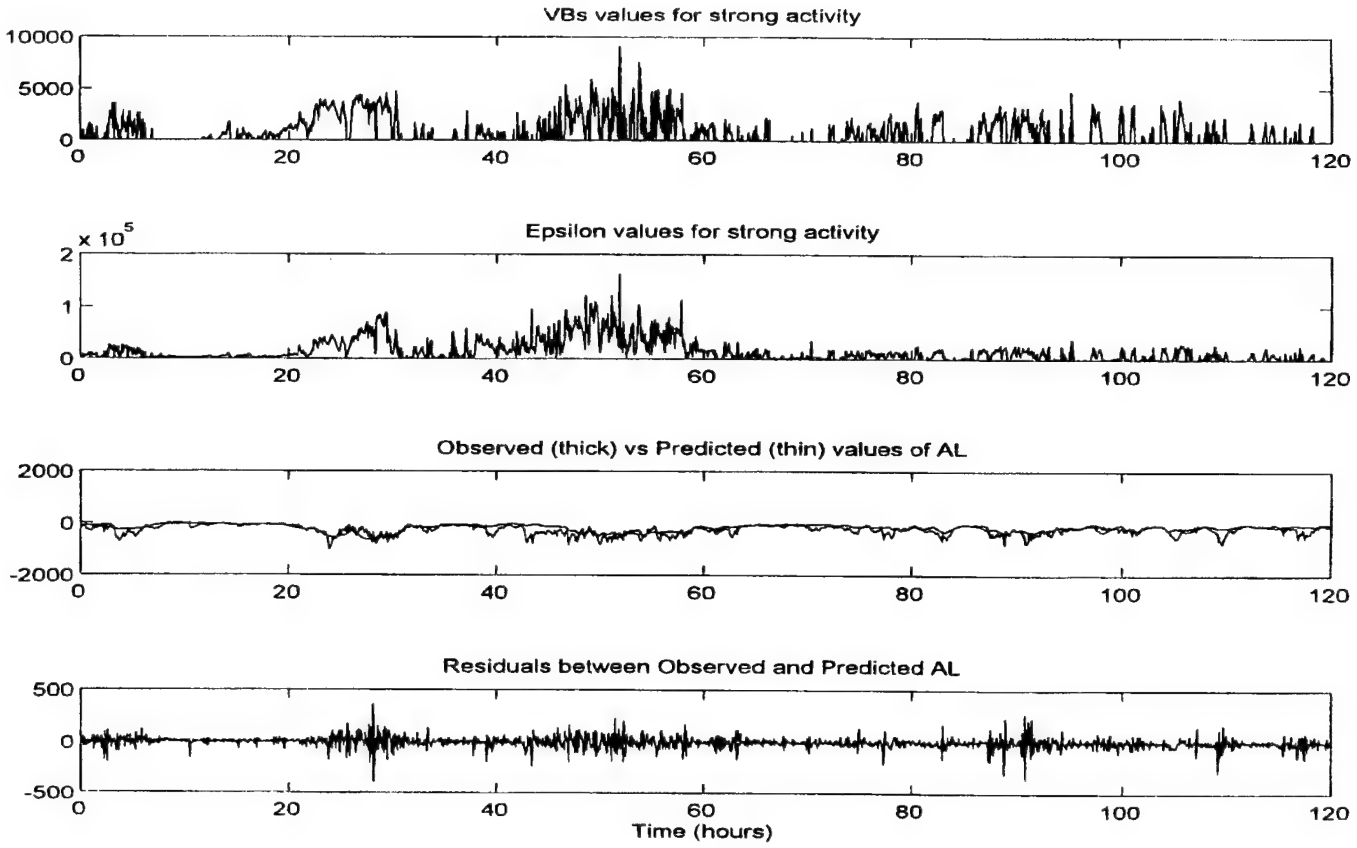

Figure C14. Multiple input model for VBs and Epsilon (strong activity).

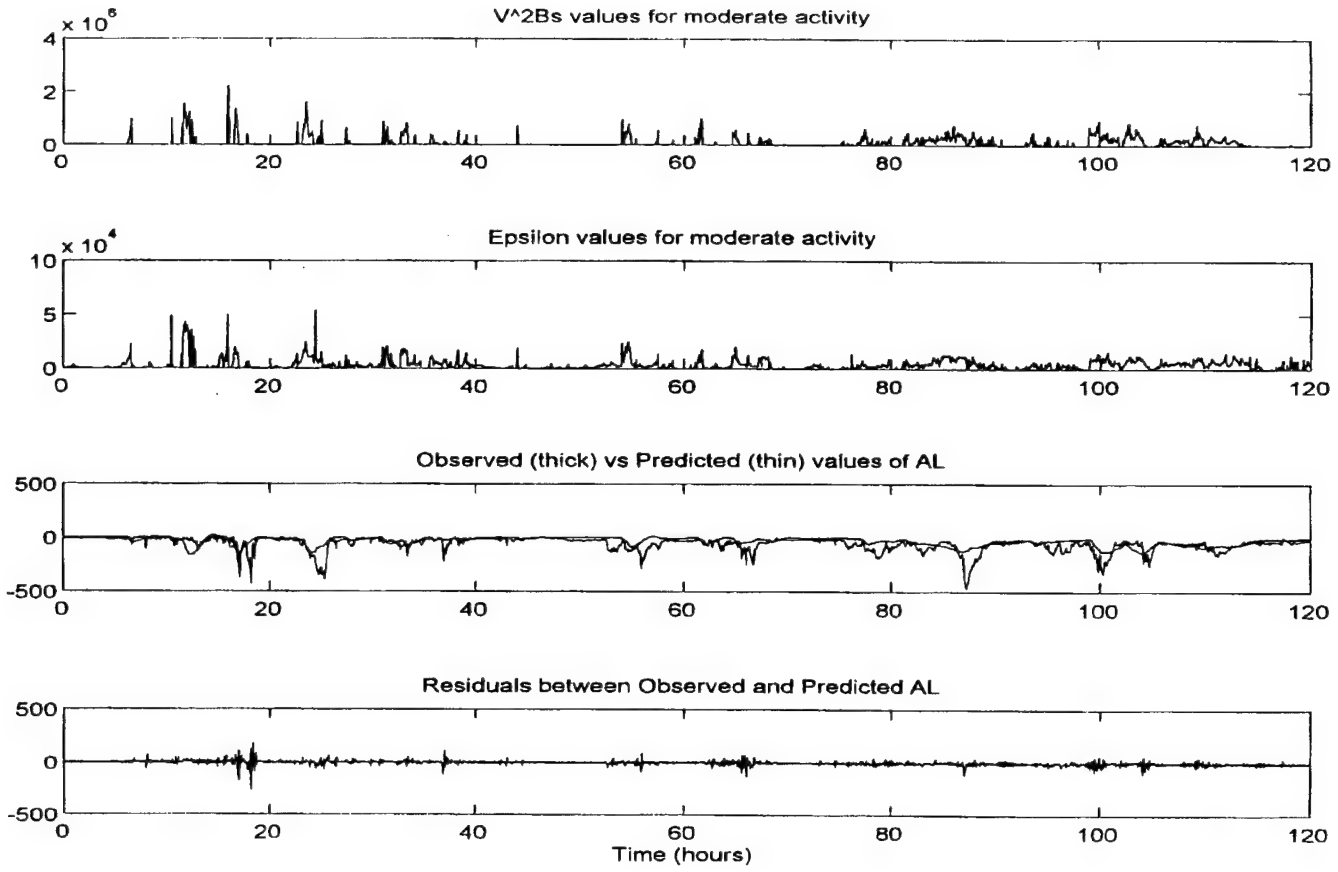

Figure C15. Multiple input model for V^2Bs andEpsilon (moderate activity).

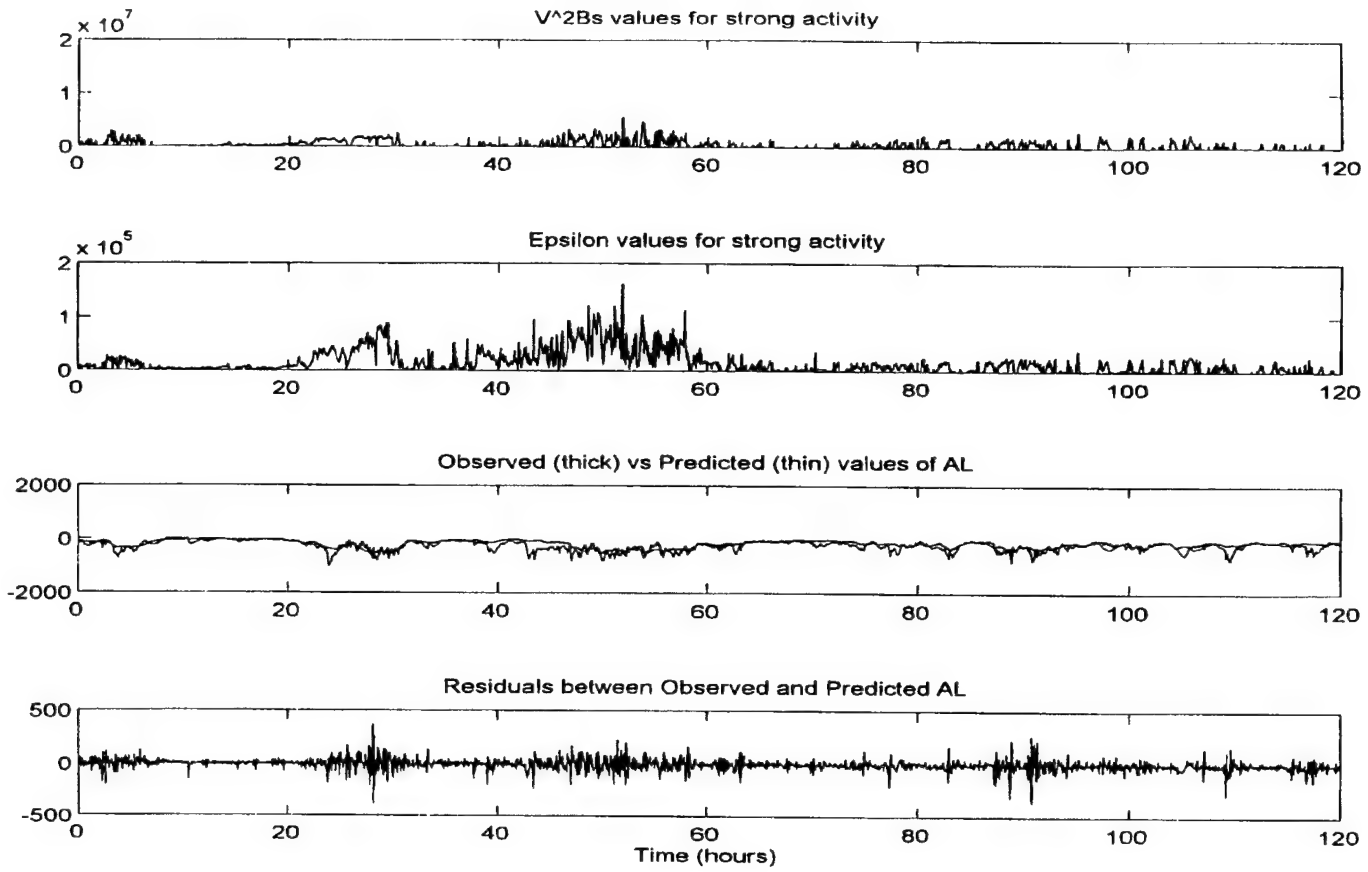

Figure C16. Multiple input model for VBs and Epsilon (strong activity).

Appendix D: Correlation Values

Correlations between input and AL for models used

	Bargatze	Linear Prediction Filtering			Vassiliadis
	Single	Single	Dual	Triple	State-Input
Interval	Input	Input	Input	Input	Space
1	68	68	82	87	84
2	79	80	87	89	91
3	43	45	49	62	86
4	0	31	51	67	79
5	42	45	61	76	88
6	59	59	66	69	93
7	64	65	71	79	96
8	65	65	74	83	92
9	44	44	75	87	91
10	79	79	82	81	93
11	65	65	72	91	91
12	63	63	72	78	88
13	61	65	71	75	94
14	87	87	91	91	97
15	73	74	80	83	93
16	76	76	82	84	95
17	68	68	73	84	94
18	61	62	70	74	84
19	64	59	55	80	96
20	74	74	77	79	95
21	84	84	87	89	96
22	57	58	70	74	96
23	60	60	72	78	95
24	79	79	84	87	96
25	48	64	70	74	92
26	54	56	66	69	90
27	81	81	82	83	95
28	73	73	78	80	94
29	60	60	66	73	94
30	68	68	75	76	93
31	84	84	86	66	93
32	73	74	76	86	94
33	72	73	73	75	94
34	72	72	82	86	92

The values listed are percentages of one, where 100 indicates a perfect or complete correlation with the output data.

Appendix E: Bargatze's Stack Plot of Filters

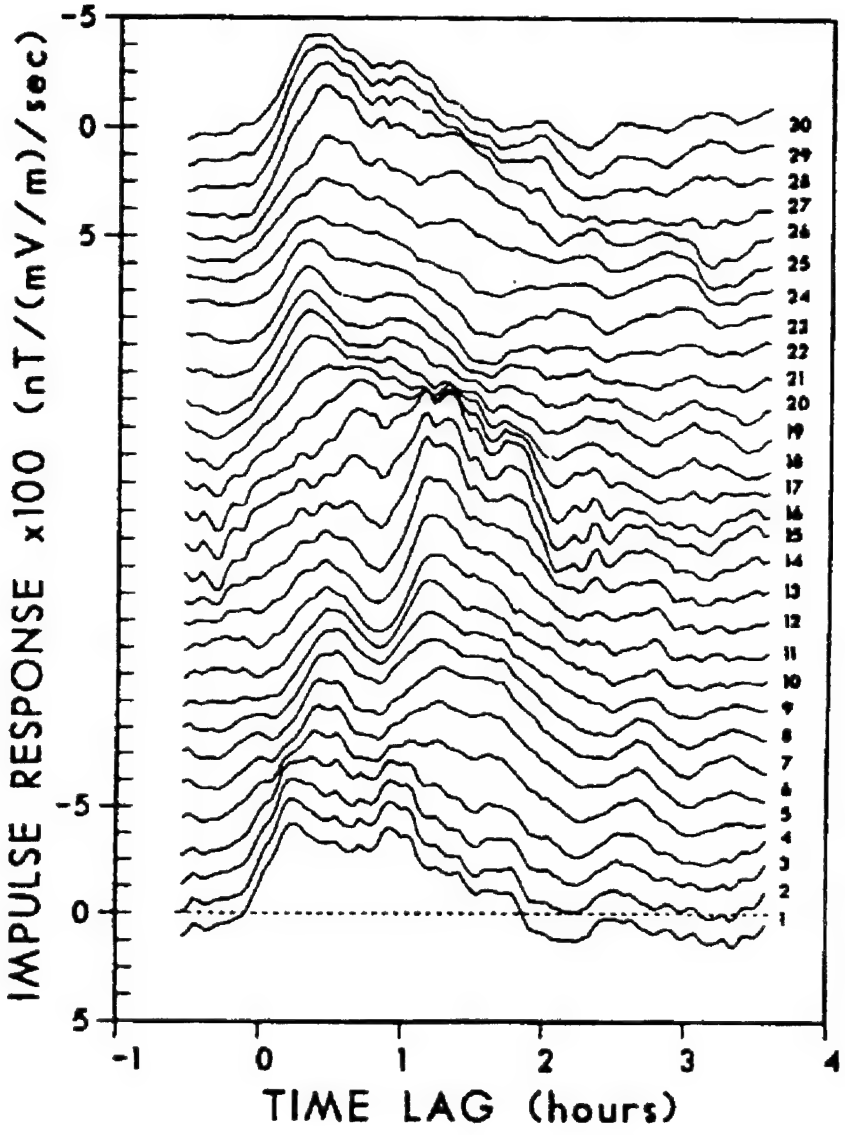

Figure E1. Stack plot of linear prediction filters for all levels of geomagnetic activity. (Adapted from Bargatze [1985:6389])

Bibliography

Air Force Institute of Technology. Style guide for Theses and Dissertations. Wright-Patterson AFB, OH: September, 1994.

Air Force Material Command. Handbook of Geophysics and the Space Environment. Edited by Adolph S. Jursa. Air Force Geophysics Laboratory, 1985.

Arnoldy, R. L., "Signature in the interplanetary medium for substorms," Journal of Geophysical Research, 76 (22): 5189 (1971).

Bargatze, L. F., D. N. Baker, R. L. McPherron, and E. W. Hones, Jr. "Magnetospheric Impulse Response for Many Levels of Geomagnetic Activity," Journal of Geophysical Research, 90, A7: 6387:6394 (July 1, 1985)

Baumjohann, Wolfgang. "Merits and Limitations of the Use of Geomagnetic Indices in Solar Wind-Magnetosphere Coupling Studies," Solar Wind-Magnetosphere Coupling, Edited by Y. Kamide and J. A. Slavin, 3-15 (1986)

Berthelier, Annick. "The Geomagnetic Indices: Derivation, Meaning, and Uses in Solar-Terrestrial Physics," Solar-Terrestrial Predictions Proceedings IV, Volume 3, Edited by J. Hruska, M. A. Shea, D. F. Smart, and G. Heckman: 3-20. Boulder CO: Dept. Of Commerce, September 1993.

Clauer, C. Robert. "The Technique of Linear Prediction Filters Applied to Studies of Solar Wind-Magnetosphere Coupling," Solar Wind-Magnetosphere Coupling, Edited by Y. Kamide and J. A. Slavin, 39-57 (1986).

Cliver, Ed. Research Scientist, Geophysics Laboratory, Hanscom AFB, MA. Personal Correspondence. January-September 1995.

Davis, T. N., and M. Sugiura. "Auroral electrojet activity index AE and its universal time variations", Journal of Geophysical Research., 71: 785-801 (1966).

Department of the Air Force. SWIM User's Guide and Reference. Hanscom AFB: Phillips Laboratory/Geophysics Directorate, 1995.

Gehred, P. A., W. Cliffswallow, and J. D. Schroeder III. A Comparison of USAF Ap and Kp Indices to Gottingen Indices. NOAA Technical Memorandum ERL SEL-88. Boulder CO:Space Environment Laboratory, March 1995.

Gonzalez, W. D. " Unified view of Solar Wind-Magnetosphere Coupling Functions," Planetary and Space Science: 38, 5: 627-632 (1990).

Hargreaves, J.K. The solar-terrestrial environment. Cambridge: University Press, 1992.

Kamide, Y., and W. Baumjohann, "Estimation of electric field and currents from IMS magnetometer data for the CDAW-6 intervals: Implications for substorm dynamics," Journal of Geophysical Research, 90: 1305-1317 (1985).

Kelley, Michael C. The Earth's Ionosphere: Plasma Physics and Electrodynamics. New York: Academic Press, 1989.

Klimas, Alexander J. Research Scientist, Goddard Space Flight Center, NASA. Personal Correspondence. August-September 1995.

Klimas, A. J., D. N. Baker, D. Vassiliadis, and D. A. Roberts. "Substorm recurrence during steady and variable solar wind driving: Evidence for a normal mode in the unloading dynamics of the magnetosphere," Journal of Geophysical Research, 90 (A8): 14855-14861 (1994).

Klimas, A. J., D. N. Baker, D. A. Roberts, and D. H. Fairfield. "A nonlinear Dynamic Analogue Model of Substorms," Geophysical Monograph 64: 449-459 (1991).

Ljung, Lennart. System Identification Toolbox User's Guide. Version 4.0, UNIX. Computer software and tutorial. The MathWorks, Inc., Natick MA, 1992.

Makridakis, Spyros, and Steven C. Wheelwright. Interactive Forecasting: Univariate and Multivariate Methods. 2nd Ed. Holden-Day: San Fransisco, 1978.

Matlab: High-Performance Numeric Computation and Visualization Software. Version 4.0, UNIX. Computer software. The MathWorks, Inc., Natick MA, 1992.

Menvielle, M. And A. Berthelier. "The *K*-derived Planetary indices: Description and Availability," Reviews of Geophysics, 29, 3: 415-432 (August 1991).

Nostrand, Philip M. Forecast Verification of the 10.7 Centimeter Solar Flux and the Ap Daily Geomagnetic Activity Indices. MS thesis, AFIT/GSO/PH-OS/84D-2. School of Engineering, Air Force Institute of Technology (AU), Wright-Patterson AFB OH, December 1984.

Parks, George K. Physics of Space Plasmas: An Introduction. New York: Addison-Wesley Publishing Company, 1991.

Perreault, P., and S.-I. Akasofu, "A study of geomagnetic storms," Geophysical Journal J. R. Astronomical Society., 54: 547 (1978).

Plasma Physics: An introductory course. Ed. R. O. Dendy. Cambridge: University Press, 1993.

Robinson, Enders A. Multichannel time series analysis with Digital Computer Programs. Holden-Day: San Fransisco, 1967.

Rostoker, Gordon. "Magnetospheric Substorms-Their phenomenology and predictability." Solar-Terrestrial Predictions Proceedings IV, Volume 3, Edited by J. Hruska, M. A. Shea, D. F. Smart, and G. Heckman: 21-35. Boulder: CO: Dept. of Commerce, September 1993.

Russell, C. T. "Solar Wind Control of Magnetospheric Configuration," Solar Wind-Magnetosphere Coupling, Edited by Y. Kamide and J. A. Slavin, 209-231 (1986).

Smart, D. F., Research Scientist. Geophysics Laboratory, Hanscom AFB, MA. Personal Correspondence. January-July 1995.

Tascione, Thomas F. Introduction to the Space Environment. Malabar, Florida: Orbit Book Company, 1994.

Vassiliadis, D., A. J. Klimas, D. N. Baker, and D. A. Roberts. "A description of the solar wind-magnetosphere coupling based on nonlinear filters," Journal of Geophysical Research, 100, A3: 3495-3512 (March 1, 1995).

Weidner, Richard T. Physics. Boston: Allyn and Bacon, 1985.

REPORT DOCUMENTATION PAGE

Form Approved
OMB No. 0704-0188

1. AGENCY USE ONLY *(Leave blank)*	2. REPORT DATE	3. REPORT TYPE AND DATES COVERED
	January 1996	Master's Thesis

4. TITLE AND SUBTITLE
Application of Autoregressive Moving Average Linear Prediction Filters to the Characterization of Solar Wind-Magnetosphere Coupling

5. FUNDING NUMBERS

6. AUTHOR(S)
Carter N. Borst, Capt, USAF

7. PERFORMING ORGANIZATION NAME(S) AND ADDRESS(ES)
Air Force Institute of Technology, WPAFB OH 45433-6583

8. PERFORMING ORGANIZATION REPORT NUMBER

9. SPONSORING / MONITORING AGENCY NAME(S) AND ADDRESS(ES)
Ed Cliver
PL/GPSG
29 Randolph Rd
Hanscom AFB, MA 01731-3010

10. SPONSORING / MONITORING AGENCY REPORT NUMBER

11. SUPPLEMENTARY NOTES

12a. DISTRIBUTION / AVAILABILITY STATEMENT
Approved for public release; distribution unlimited

12b. DISTRIBUTION CODE

13. ABSTRACT *(Maximum 200 words)*

Linear prediction filtering techniques have been used in studying the coupling processes between the solar wind and magnetosphere. The magnetosphere is a complex, dynamic system with at least two independent coupling methods for energy input, driven and unloading. Linear models were built and tested on the Bargatze data set, consisting of over 70 days of geomagnetic indices and solar wind data ordered in 34 intervals of increasing geomagnetic activity. Linear filtering techniques employing single- and multiple-input, autoregressive models predicted values of the magnetic index AL from solar wind data. The impulse response curves of the AL-coupling function groups showed amplitude peaks at 25 and 70 minutes, confirming results in previous studies. The separate peaks indicate responses corresponding to the driven and unloading time scales. The average correlation coefficients generated between predicted AL values and the measured values of AL were 0.665, 0.738, and 0.793 for single, dual, and triple input models, respectively.

14. SUBJECT TERMS	15. NUMBER OF PAGES
Magnetosphere, Solar wind, Geomagnetic activity, Prediction filters Linear filters, magnetospheric coupling	104
	16. PRICE CODE

17. SECURITY CLASSIFICATION OF REPORT	18. SECURITY CLASSIFICATION OF THIS PAGE	19. SECURITY CLASSIFICATION OF ABSTRACT	20. LIMITATION OF ABSTRACT
Unclassified	Unclassified	Unclassified	UL

GENERAL INSTRUCTIONS FOR COMPLETING SF 298

The Report Documentation Page (RDP) is used in announcing and cataloging reports. It is important that this information be consistent with the rest of the report, particularly the cover and title page. Instructions for filling in each block of the form follow. It is important to ***stay within the lines*** to meet ***optical scanning requirements***.

Block 1. Agency Use Only *(Leave blank)*.

Block 2. Report Date. Full publication date including day, month, and year, if available (e.g. 1 Jan 88). Must cite at least the year.

Block 3. Type of Report and Dates Covered. State whether report is interim, final, etc. If applicable, enter inclusive report dates (e.g. 10 Jun 87 - 30 Jun 88).

Block 4. Title and Subtitle. A title is taken from the part of the report that provides the most meaningful and complete information. When a report is prepared in more than one volume, repeat the primary title, add volume number, and include subtitle for the specific volume. On classified documents enter the title classification in parentheses.

Block 5. Funding Numbers. To include contract and grant numbers; may include program element number(s), project number(s), task number(s), and work unit number(s). Use the following labels:

C	- Contract	**PR**	- Project
G	- Grant	**TA**	- Task
PE	- Program Element	**WU**	- Work Unit Accession No.

Block 6. Author(s). Name(s) of person(s) responsible for writing the report, performing the research, or credited with the content of the report. If editor or compiler, this should follow the name(s).

Block 7. Performing Organization Name(s) and Address(es). Self-explanatory.

Block 8. Performing Organization Report Number. Enter the unique alphanumeric report number(s) assigned by the organization performing the report.

Block 9. Sponsoring/Monitoring Agency Name(s) and Address(es). Self-explanatory.

Block 10. Sponsoring/Monitoring Agency Report Number. *(If known)*

Block 11. Supplementary Notes. Enter information not included elsewhere such as: Prepared in cooperation with...; Trans. of...; To be published in.... When a report is revised, include a statement whether the new report supersedes or supplements the older report.

Block 12a. Distribution/Availability Statement. Denotes public availability or limitations. Cite any availability to the public. Enter additional limitations or special markings in all capitals (e.g. NOFORN, REL, ITAR).

- **DOD** - See DoDD 5230.24, "Distribution Statements on Technical Documents."
- **DOE** - See authorities.
- **NASA** - See Handbook NHB 2200.2.
- **NTIS** - Leave blank.

Block 12b. Distribution Code.

- **DOD** - Leave blank.
- **DOE** - Enter DOE distribution categories from the Standard Distribution for Unclassified Scientific and Technical Reports.
- **NASA** - Leave blank.
- **NTIS** - Leave blank.

Block 13. Abstract. Include a brief *(Maximum 200 words)* factual summary of the most significant information contained in the report.

Block 14. Subject Terms. Keywords or phrases identifying major subjects in the report.

Block 15. Number of Pages. Enter the total number of pages.

Block 16. Price Code. Enter appropriate price code *(NTIS only)*.

Blocks 17. - 19. Security Classifications. Self-explanatory. Enter U.S. Security Classification in accordance with U.S. Security Regulations (i.e., UNCLASSIFIED). If form contains classified information, stamp classification on the top and bottom of the page.

Block 20. Limitation of Abstract. This block must be completed to assign a limitation to the abstract. Enter either UL (unlimited) or SAR (same as report). An entry in this block is necessary if the abstract is to be limited. If blank, the abstract is assumed to be unlimited.